THE ASTROPHYSICAL JOURNAL, 418:208–228, 1993 November 20

SPECTROSCOPY OF GIANTS IN THE SEXTANS DWARF SPHEROIDAL GALAXY

NICHOLAS B. SUNTZEFF
Cerro Tololo Inter-American Observatory, National Optical Astronomy Observatories,[1] Casilla 603, La Serena, Chile
MARIO MATEO
The Observatories of the Carnegie Institution of Washington, 813 Santa Barbara Street, Pasadena, CA 91101
DONALD M. TERNDRUP[2]
Department of Astronomy, The Ohio State University, Columbus, OH 43210
EDWARD W. OLSZEWSKI
Steward Observatory, University of Arizona, Tucson, AZ 85721
AND
DOUG GEISLER AND W. WELLER
Cerro Tololo Inter-American Observatory, National Optical Astronomy Observatories,[1] La Serena, Chile
Received 1992 December 14; accepted 1993 April 26

ABSTRACT

We have obtained spectra in the region of the Ca II infrared triplet at 8500 Å for 80 stars in the direction of the Sextans dwarf spheroidal galaxy. We have found 43 radial velocity members of the Sextans galaxy and 36 field stars. The mean velocity of the Sextans galaxy is 227.9 ± 1.8 km s^{-1}, in agreement with the previously determined value of 230 ± 6 km s^{-1} from Da Costa et al. (1991). We find that the intrinsic velocity dispersion of Sextans is 6.2 ± 0.9 km s^{-1} based on 33 stars. The two standard methods for estimating the total mass-to-light ratio yield $(M/L)_{\rm tot} = 54^{+44}_{-24}$ and 30^{+20}_{-13}, implying significant amounts of dark matter are present, although we cannot rule out binary contamination as the cause of the large observed velocity dispersion with only a single epoch of observations. The mean metallicity of Sextans is $\langle$[Fe/H]$\rangle = -2.05 \pm 0.04$, with an intrinsic star-to-star metallicity dispersion of 0.19 ± 0.02 dex in [Fe/H]. The abundance measurements based on the Ca II line strengths are found to be correlated with the color of the star, supporting the existence of a real metallicity dispersion. The mean metallicity is in excellent agreement with the general trend of metallicity–absolute galaxian magnitude for the dwarf spheroidal galaxies that are satellites to the Milky Way galaxy. The horizontal branch of Sextans is quite red for the derived mean metallicity implying that Sextans, like Draco, is a "second parameter" object that may be a few Gyr younger than the typical Galactic globular cluster.

Subject headings: galaxies: abundances — galaxies: kinematics and dynamics — galaxies: stellar content — stars: giant

1. INTRODUCTION

Both the Milky Way and Andromeda galaxies have a small number of faint satellite galaxies with $M_V < -14$ that are apparently gravitationally bound to the main galaxy. These galaxies, often called *dwarf spheroidal* (dSph) galaxies, are important probes of dark matter (Aaronson & Olszewski 1988; Zaritsky et al. 1989) and theories of the formation of galaxies (Searle & Zinn 1978). The number of these objects is small, and any new candidate dSph galaxy is an important addition to the understanding of how galaxies form.

With the discovery of a dSph galaxy in Sextans (Irwin et al. 1990), the total number of such objects around the Galaxy is now eight. Two papers have already appeared since the discovery paper discussing the general characteristics of the galaxy. Da Costa et al. (1991) report a mean velocity and mean metallicity for the galaxy, and Mateo et al. (1991a) present a deep color-magnitude diagram. These studies show that Sextans is similar to the other well-studied lowest luminosity dSph galaxies, Draco and Ursa Minor. The galaxy is metal-poor at [Fe/H] ~ -1.7 and is evidently composed only of very old (ages greater than 12 Gyr) stars. The mean galactocentric velocity of Sextans of 80 km s^{-1} is similar to the other dSph galaxies and outer halo globular clusters, which implies that Sextans is also bound to the Galaxy.

These previous papers have left a number of questions unanswered. We would like to know, in analogy to Draco and Ursa Minor, if Sextans has a "large" or "small" velocity dispersion with respect to the predicted dispersion from King model fits to the stellar distribution, and if there is a significant star-to-star dispersion in metallicity. In addition, the basic data of the mean heliocentric velocity and abundance should be verified and improved upon, especially in the case of the abundances where it was found that Sextans is significantly more metal-rich than the other dSph galaxies at the same luminosity.

In this paper we present abundances and velocities for 43 giants in the Sextans dSph galaxy observed with the Argus fiber positioning system at the CTIO 4 m telescope. In § 2 we discuss the observations, data reduction procedures, and the measurement of the velocities and metallicities. In § 3 we calculate the intrinsic velocity dispersion, and in § 4, we calculate both the mean and intrinsic metallicity dispersion. Section 4 concludes with a brief discussion relating the metallicity characteristics of Sextans to models of chemical enrichment of galaxies. In § 5 we derive the M/L ratio for Sextans.

[1] The National Optical Astronomy Observatories are operated by the Association of Universities for Research in Astronomy, Inc., under cooperative agreement with the National Science Foundation.
[2] Presidential Young Investigator.

2 OBSERVATIONS AND REDUCTIONS

2.1. *Photometry*

Because of the low surface density of Sextans, it is crucial to choose carefully the spectroscopic candidates to avoid being overwhelmed by foreground field stars. Consequently, we obtained CCD photometry of a 630 arcmin^2 region centered on Sextans (based on the position given by Irwin et al. 1990) in order to identify possible Sextans members for subsequent spectroscopic study. These data were obtained at the Las Campanas Observatory of the Carnegie Institution of Washington in a single run in 1991 March that ended about 1 week prior to the spectroscopic run. These data were also used as the basis for the positions used for the subsequent Argus observations. The data were obtained on the Swope 1 m telescope equipped with a thinned Tektronics 1024 × 1024 CCD using Johnson *BV* filters. The entire mosaicked CCD field is shown in Figure 1 (Plate 4), and Figure 2 illustrates the resulting color-magnitude (*C-M*) diagram of about 3400 objects measured in the region. Although badly affected by field star contamination, Figure 2 reveals a clear red giant and subgiant branch and a predominantly red horizontal branch.

The spectroscopic candidates were chosen to lie in a sloping band about 0.4 mag wide in $(B-V)$ extending toward brighter magnitudes from the red giant clump [located at $V \sim 20.35$, $(B-V) \sim 0.6$] and enclosing the giant branch which is visible as a slight enhancement in the *C-M* diagram running diagonally from the red horizontal branch region to $V \sim 17.2$, $(B-V) \sim 1.5$. We also selected all bright stars lying redward of this band to $V \sim 18$ to include any possible Sextans carbon stars in our spectroscopic sample. All the stars observed spectroscopically are listed in Table 1, where we list the coordinates, photometry, errors in the photometry, and cross-references to other studies. The error listed is the estimated parent standard deviation, and not the mean error. The uncertainties in the photometric transformations are 0.03 mag in both V and $(B-V)$.

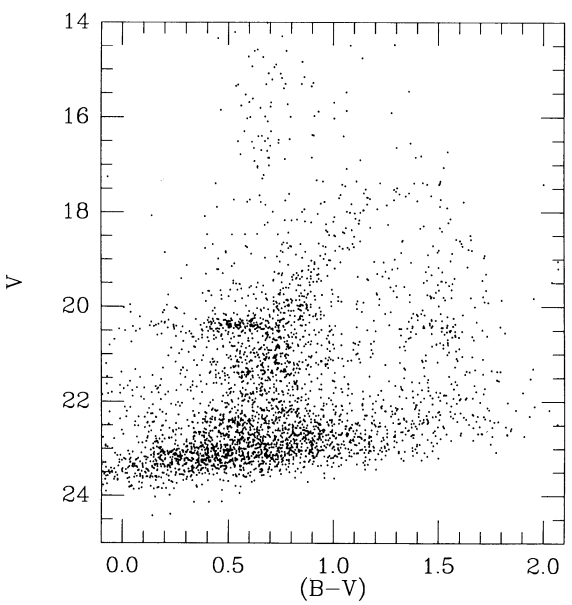

FIG. 2.—CCD photometry in *BV* for 3454 stars in a 630 arcminute^2 region centered on the Sextans dSph galaxy.

Some of the stars selected for spectroscopic study were considerably fainter than $V \sim 19$. These represent cases where the preliminary photometry available at the time of the spectroscopic observations was significantly in error, presumably due to cosmic-ray contamination or some other single-frame defect. The final photometry shown in Figure 2 results from averaging up to 15 separate frames for stars located in about 60% of the area shown in Figure 1. In any case, our spectra for the six stars with $V \sim 19$ did not yield usable results, and we shall not discuss these stars further in our analysis. Note that the *C-M* diagram is statistically incomplete at the fainter limits because not all the frames go to equal depths. For further discussion of the *C-M* diagram, we refer the reader to Mateo, Fischer, & Kzreminski (1993) where the morphology of the *C-M* diagram is analyzed and the data are used to search for variable stars.

2.2. *Argus Spectra*

We obtained spectra for the Sextans giant candidates and Galactic globular cluster members with the Argus multifiber system (Ingerson 1988; Lutz et al. 1990; Ingerson et al. 1993) on the CTIO 4 m telescope in a single observing run from 1991 March 25 to 27 (UT). The Argus fiber system allows the independent assignment of up to 24 fiber pairs across a 50′ field. The position of each fiber was checked via a periscope arrangement whereby the fiber, back-lit from the spectrograph, appears superposed on the focal plane such that the star and fiber are seen simultaneously. One fiber positioner was not working, so that we used 23 fiber pairs for the whole run.

The fibers are fed into a bench-mounted spectrograph, located in an isolated room below the observing floor. The spectrograph consists of a classical Schmidt optics collimator with focal length of 510 mm, a grating, and the CTIO red-optimized air Schmidt camera with a focal length of 229 mm. The KPGLD grating, with 790 grooves mm^{-1} and blazed at 8000 Å, was used in first order. The air Schmidt camera has a GEC CCD (384 × 576 22 μm pixels) at its focus. Since the chip has very low quantum efficiency below 5000 Å, no order-separating filter was used. The spectral dispersion was 55 Å mm^{-1}. The 100 μm fibers should project to roughly 2.1 pixels on the CCD; it was discovered during the run that the CCD was not quite tangent to the focal plane. This slight tilt of the CCD in the very fast Schmidt camera of f/0.9 degraded the focus on either side of the CCD field to about 2.5 pixels (108 km s^{-1} resolution).

A red filter was used in the television during this bright-time run. We observed near full Moon, which we later discovered was not ideal for red giants with $V > 18$ at 8500 Å. The small increase in the sky brightness (of roughly 1 mag in *I*) at full Moon noticeably increased the "continuum" level (actually scattered moonlight) of the sky and degraded the sky-subtracted spectra.

2.3. *Data Reduction Procedures for Argus Data*

Since the reduction of the fiber data is not quite standard yet, we will give a brief outline of the calibrations needed and the steps in the data reduction. All the data reduction was done with the "CCDRED" and "ARGUS" data reduction packages of IRAF.[3]

[3] IRAF is distributed by the National Optical Astronomy Observatories, which is operated by the Association of Universities for Research in Astronomy, Inc., under cooperative agreement with the National Science Foundation.

PLATE 4

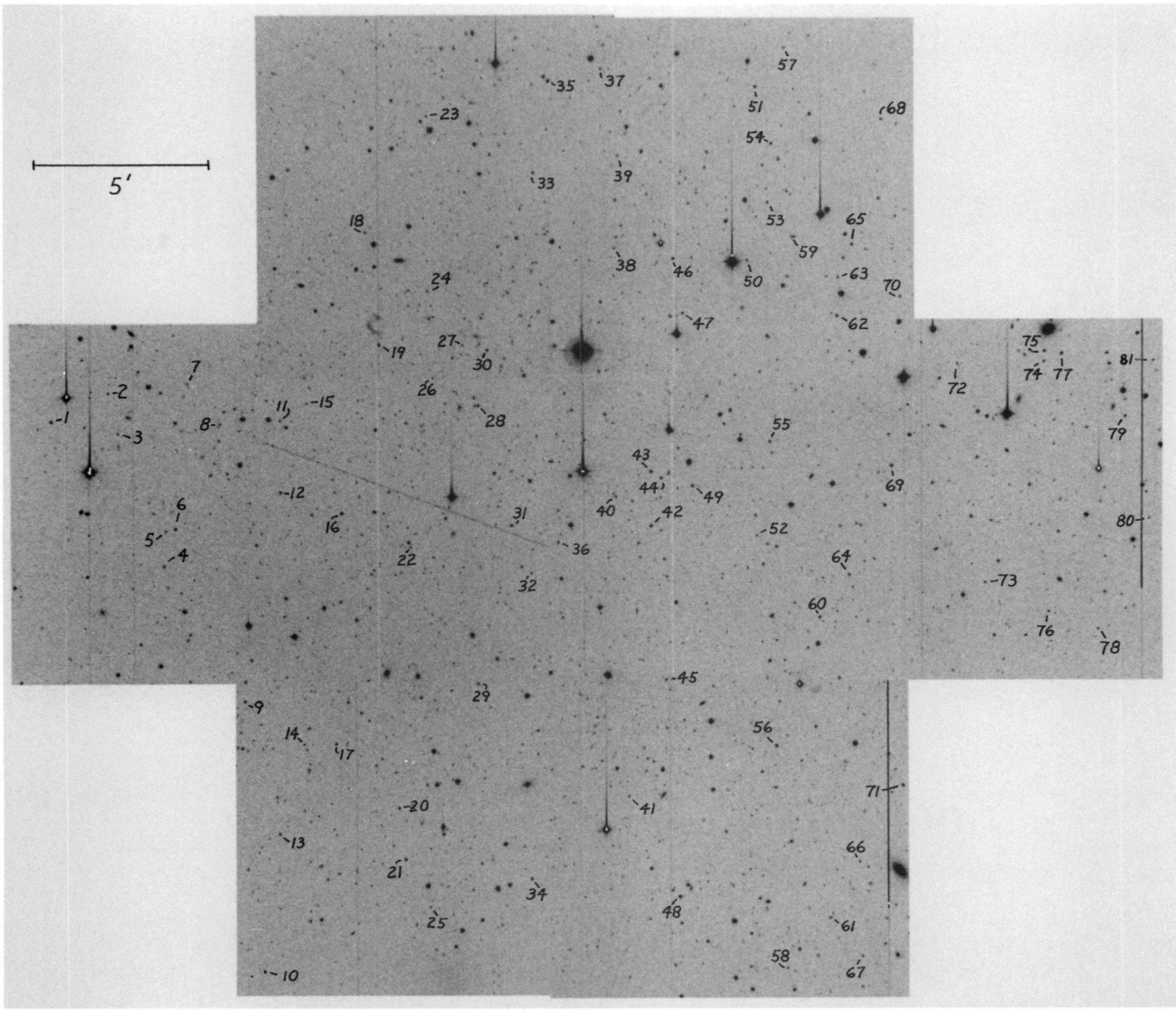

FIG. 1.—A finding chart for the spectroscopically observed stars in the Sextans field listed in Table 1. This chart was constructed from six LCO 1 m telescope *V*-band CCD images. North is to the left and east toward the top. Due to a processing error, the extreme lower left of the chart was corrupted; the location of star 10 is therefore approximate.

1993ApJ...418..208S

TABLE 1

SPECTROSCOPICALLY OBSERVED CANDIDATE MEMBERS OF THE SEXTANS DWARF GALAXY

Star	RA (2000)	Dec (2000)	V	$\sigma(V)$	$B-V$	$\sigma(B-V)$	Cross-Identification
1	10 13 18.3	−1 24 46	17.44	0.01	1.06	0.01	DC6
2	10 13 21.7	−1 26 21	18.72	0.02	1.03	0.04	
3	10 13 17.1	−1 26 39	19.02	0.02	0.99	0.04	
4	10 13 01.9	−1 27 57	17.41	0.01	1.51	0.02	
5	10 13 05.9	−1 28 01	18.24	0.01	1.12	0.03	
6	10 13 06.2	−1 28 17	17.91	0.01	1.54	0.03	
7	10 13 22.9	−1 28 35	18.64	0.01	0.76	0.03	
8	10 13 18.3	−1 29 32	18.08	0.01	1.21	0.03	
9	10 12 46.3	−1 30 16	18.32	0.01	1.18	0.03	
10	10 12 15.3	−1 30 54	17.05	0.01	1.53	0.02	
11	10 13 18.7	−1 31 14	18.17	0.01	1.13	0.03	
12	10 13 10.5	−1 31 16	17.74	0.01	1.29	0.03	
13	10 12 31.1	−1 31 17	17.65	0.01	1.47	0.02	
14	10 12 41.5	−1 31 57	18.52	0.01	1.10	0.03	
15	10 13 20.7	−1 32 00	18.73	0.02	0.80	0.04	
16	10 13 07.9	−1 32 10	18.13	0.01	1.11	0.03	
17	10 12 41.6	−1 32 52	17.59	0.01	1.36	0.02	DC13
18	10 13 40.2	−1 33 40	17.95	0.01	1.15	0.03	
19	10 13 27.3	−1 34 05	18.00	0.02	1.13	0.03	S292
20	10 12 34.3	−1 34 41	17.41	0.01	2.00	0.02	
21	10 12 28.3	−1 34 53	17.38	0.01	1.51	0.02	
22	10 13 04.2	−1 34 59	18.49	0.01	1.01	0.03	S129
23	10 13 53.6	−1 35 25	18.72	0.02	0.98	0.04	
24	10 13 33.6	−1 35 28	18.72	0.02	0.95	0.03	
25	10 12 22.8	−1 35 36	18.42	0.01	1.05	0.02	
26	10 13 23.7	−1 35 37	18.66	0.02	0.93	0.03	S273
27	10 13 27.4	−1 36 28	18.30	0.02	0.94	0.03	S286
28	10 13 20.6	−1 36 54	17.29	0.01	1.39	0.02	S242
29	10 12 48.6	−1 36 57	18.74	0.01	1.10	0.03	S17
30	10 13 26.9	−1 37 11	17.88	0.02	1.04	0.03	S279
31	10 13 06.8	−1 37 53	17.48	0.01	1.30	0.02	D241, S142
32	10 13 01.3	−1 38 27	18.74	0.01	0.88	0.03	D63, S96
33	10 13 47.2	−1 38 28	17.78	0.02	1.62	0.03	
34	10 12 26.2	−1 38 30	18.00	0.01	1.08	0.02	
35	10 13 57.7	−1 38 53	17.30	0.02	1.41	0.02	
36	10 13 04.9	−1 39 14	17.96	0.02	1.10	0.03	D161, S125
37	10 13 59.1	−1 40 22	18.45	0.02	0.96	0.03	
38	10 13 38.6	−1 40 46	18.90	0.02	0.87	0.04	
39	10 13 49.2	−1 40 51	18.77	0.02	1.00	0.04	
40	10 13 10.2	−1 40 52	18.37	0.01	1.09	0.03	D346, S166
41	10 12 35.8	−1 41 16	18.74	0.02	1.08	0.04	
42	10 13 06.8	−1 41 51	18.10	0.01	1.01	0.02	D216, S136
43	10 13 13.1	−1 41 51	17.41	0.01	1.45	0.02	D447, S190
44	10 13 12.3	−1 42 09	18.22	0.01	1.06	0.03	D418, S182
45	10 12 49.3	−1 42 19	18.77	0.02	1.05	0.04	S15
46	10 13 37.5	−1 42 27	17.99	0.04	1.54	0.05	
47	10 13 31.3	−1 42 44	18.14	0.01	1.56	0.03	
48	10 12 24.3	−1 42 44	16.72	0.01	1.55	0.02	
49	10 13 11.5	−1 43 02	17.59	0.01	1.15	0.02	D394, S176, DC17
50	10 13 37.4	−1 44 33	18.83	0.02	0.87	0.03	
51	10 13 57.2	−1 44 46	17.85	0.02	1.26	0.03	
52	10 13 05.8	−1 44 52	18.50	0.01	1.01	0.03	
53	10 13 44.0	−1 45 08	17.76	0.01	1.40	0.02	
54	10 13 50.7	−1 45 13	17.51	0.01	1.29	0.02	DC15
55	10 13 16.7	−1 45 14	17.34	0.01	1.51	0.02	
56	10 12 41.8	−1 45 28	17.37	0.01	1.43	0.02	DC5
57	10 14 01.6	−1 45 34	18.79	0.02	1.08	0.04	
58	10 12 16.1	−1 45 49	17.69	0.01	1.17	0.02	
59	10 13 40.1	−1 45 50	17.61	0.01	1.32	0.02	
60	10 12 56.5	−1 46 41	17.38	0.01	1.39	0.03	
61	10 12 21.9	−1 47 01	18.02	0.01	1.10	0.02	
62	10 13 31.1	−1 47 07	17.52	0.02	1.45	0.03	
63	10 13 35.5	−1 47 08	18.37	0.02	1.20	0.03	
64	10 13 01.4	−1 47 31	17.87	0.02	1.51	0.04	
65	10 13 39.2	−1 47 32	17.29	0.01	1.31	0.02	
66	10 12 28.4	−1 47 51	18.48	0.01	0.98	0.02	
67	10 12 17.5	−1 47 57	18.33	0.01	1.06	0.02	
68	10 13 53.6	−1 48 20	18.65	0.02	1.04	0.04	
69	10 13 14.0	−1 48 42	16.84	0.01	1.40	0.02	
70	10 13 33.3	−1 48 54	17.86	0.02	1.53	0.04	
71	10 12 37.3	−1 49 05	17.55	0.01	1.30	0.02	
72	10 13 25.7	−1 50 33	18.38	0.01	0.97	0.03	
73	10 13 00.6	−1 51 23	18.25	0.01	0.97	0.02	
74	10 13 26.0	−1 52 59	17.73	0.02	1.51	0.02	
75	10 13 27.2	−1 53 00	17.38	0.01	1.22	0.02	
76	10 12 57.2	−1 53 11	18.76	0.02	0.79	0.03	
77	10 13 26.9	−1 53 29	16.54	0.02	1.37	0.02	
78	10 12 55.4	−1 54 35	18.55	0.02	1.12	0.04	
79	10 13 19.8	−1 55 17	17.93	0.02	1.21	0.03	
80	10 13 08.1	−1 56 00	18.72	0.02	0.80	0.03	
81	10 13 26.2	−1 56 03	18.67	0.02	1.09	0.04	

NOTE.—The letters D and S precede the numbers from Tables 4 and 6, respectively, of Mateo et al. 1991a, while DC precedes the ID numbers used by Da Costa et al. 1991.

A nightly average of the bias structure was calculated by averaging 25 zero s exposures. No "preflash" correction was made to the data, since the CTIO CCD laboratory tests on the chip showed minimal charge transfer inefficiency at low light levels. Because the bias structure was purely due to the DC variations in the serial register, the bias data were averaged along "lines" (where a line is the direction of the read in the serial register) to produce a one-dimensional bias line. The program data were subtracted by the average DC level in the overscan region, trimmed, and every line was subtracted by the bias line.

We created a two-dimensional flat-field by placing a diffusing glass filter in front of the fiber tail assembly at the focus of the collimator, and observing the daytime sky. The diffusing glass is thick enough that the variations in intensity both due to the fiber point-spread function (psf) perpendicular to the dispersion and the solar spectral lines along the dispersion are washed out. This flat-field has roughly the right color of the normal dispersed spectra. The flat was normalized to a value of 1.0 everywhere by fitting a two-dimensional surface to the flat. This flat was divided into all the data, including the twilight sky and dome quartz flat observations. This will be a good flat-field calibration provided that there are no strong color terms or monochromatic fringing associated with the CCD.

The other basic calibrations taken were nightly observations of the dome white spot illuminated by a quartz lamp ("dome quartz flats"), the white spot illuminated by an argon-neon lamp ("dome neon flats"), and the twilight sky. During the night, after each exposure of a program field, the fibers were brought to their central position and an exposure of a neon lamp projected via a fiber-optic cable was made ("comparison lamps").

The objects were verified by observing the fibers and object field via a periscope, and if necessary, the fibers moved onto the stars. For the Sextans fields, the fibers were centered by eye. Typical exposures for the globular clusters were 2–15 minutes, and for Sextans, 30–45 minutes. Due to an undiagnosed problem on this run of flexure in the guide television camera, the fibers would drift off by up to 2″ in 40 minutes, thus limiting our longest exposure to that time.

All the data were extracted to one-dimensional spectra using the Argus reduction package in IRAF. Apertures down to about the 5% level were used to try to include all the light in each fiber, and the optimal extraction scheme was used to reduce the larger read noise introduced by using a large aperture. All apertures for a given frame were chosen to be the same size to allow simple median filtering of the sky for the sky subtraction.

The extracted dome quartz flats and twilight flats showed that there are fiber-to-fiber variations of up to 35%. The division of the *extracted* twilight flats by the extracted dome quartz flats should give the same average flux in all fibers if the light from the dome flats is really a correct representation of a parallel beam. In fact, the extracted dome flats were the same as the twilight flats to an rms of 1.5%. We corrected the extracted dome flats by these small differences and divided all the extracted data by the extracted dome quartz flats.

Note that we have flat-fielded the data twice, first by a two-dimensional flat, and second by the extracted dome quartz flat (which itself had been flattened by the two-dimensional flat) corrected to the twilight sky. This procedure is required because the spectra shift slightly perpendicular to the dispersion during the night by up to 0.3 pixels and occasionally by 1 pixel. Had we merely extracted all the data before the division by the two-dimensional flat and divided all the extracted data by the extracted quartz, significant pixel-to-pixel variations could remain in the data since the quartz spectrum could have lain at a slightly different position on the chip when compared to the program spectra.

Due to the pincushion distortion from the prime focus corrector, the fibers located near the edge of the field will sample an area of sky that is 10% less than the same fiber in the center of the field. We corrected for the real distortions using the formulae given in Chiu (1976) and Cudworth & Rees (1991).

By examining the subtraction of sky spectra from other sky spectra, it was determined that the only accurate wavelength solution was based either on the night sky emission lines or the dome neon flats. The solutions based on the internal comparison lamps introduced artificial wavelength shifts, most likely due to the fact that the internal illumination system does not bring the light in at exactly the f-ratio of the 4 m telescope prime focus. Since the shifts along the dispersion were less than 0.1 pixel per night and less that 0.2 pixels for the whole run, we used the extracted dome neon spectra to produce a set of 46 wavelength solutions for each night. All the data were then corrected by these nightly solutions. To take out the very small spectral drifts, we co-added the comparison spectra of a given observation into a one-dimensional spectrum and calculated a single shift per observation. We then applied this shift to all 46 spectra. The final, and most critical, step in the data reduction, is the sky subtraction. The Ca II infrared triplet lines lie on top of OH and O_2 night sky emission lines, which can be up to 20 times brighter than the feature of interest. As noted above, there was a small focus change across the chip. This precluded the use of a grand median of all 23 sky spectra to make a single sky spectrum. Instead, we used a running average (clipped at 3 σ) of the six sky spectra nearest the object spectrum to make a sky spectrum. Prior to the average, all the individual sky spectra were examined to exclude spectra contaminated by field stars or especially strong cosmic rays (which confused the optimal extractor described above).

It was discovered at this point that the sky and object fibers appeared to have random throughput variations of about 2% rms, probably due to the very small bending of the fibers at different positions in the field. In a very few cases there were variations as large as 6%. There was also evidence in a few cases that the fibers changed their sensitivity as a function of *color*. Because these effects were unpredictable, after the initial sky subtraction, we added or subtracted 1% of the median sky until the best subraction was made, based on the residuals of the night sky lines. The subtractions were generally good to 1.5% of the sky flux all across the spectrum. Part of this error is also due to the fact that we had to linearize the data (in wavelength) before sky subtraction. Tests done on artificial data showed that the linearization produced residuals of up to 1%. We did not attempt to take out the variations due to the color transmission variations.

For the faint spectra of the stars in the Sextans field, multiple spectra were co-added to form the final spectrum. The co-addition was weighted by our estimate of the S/N in the continuum, and spectra where cosmic rays affected any of the Ca II triplet lines were excluded from the co-addition. The final spectra for the stars in the Sextans field are the co-addition of two to eight spectra, with four spectra being typical. Thus a "typical" spectrum represents a 3 hr integration.

2.4. *Measurement of the Pseudo–Equivalent Widths*

The pseudo–equivalent widths (pseqw's) of the three Ca II infrared triplet lines were measured using the same procedure as given in Olszewski et al. (1991). The lines were fitted with Gaussian functions where the height and width are free parameters, but the line position is fixed by the known wavelength of the lines and the stellar geocentric velocity. The wavelengths of the Ca II lines and the bandpasses used are given in Olszewski et al. (1991).

Olszewski et al. (1991) used the sum of all three pseqw's as a function of the average monochromatic magnitude at 8600 Å (as measured from the long-slit spectra) to derive abundances. Since the magnitudes from the fiber spectra are somewhat poorer and the quality of the pseqw of the weakest Ca II triplet line is poor, we have decided to use the sum of the two strongest triplet lines at 8542 Å and 8662 Å (called $W_{8542} + W_{8662}$ or W for short) as suggested by Armandroff & Da Costa (1991, hereafter AD2).

For the six globular clusters where we had multiple exposures of high signal-to-noise ratio, repeat W values agree to 0.09 Å rms, implying an average error of 0.06 Å per observation. For M11 which was observed each night, the average difference of the nightly zero point of W was less than 0.02 Å. The estimated error for the three observations of the M11 stars was 0.06 Å for a single observation, the same as for the globular cluster stars. For the seven stars in NGC 6397 and NGC 6752 in common with the AD2 results, the mean difference (in the sense of this work *minus* AD2), estimated parent standard deviation of the difference, and number of stars in common are (−0.11 Å, 0.09 Å, 7). This difference excludes star A12 in NGC 6752 which was near saturation. A comparison of cluster giants in common with the Armandroff, Da Costa, & Zinn (1992, hereafter ADZ) work yields (−0.25 Å, 0.12 Å, 16), and with the Da Costa, Armandroff, & Norris (1992) work, (−0.01 Å, 0.11 Å, 10). Using the abundance calibration given in AD2, we find that these small differences between measured pseqw's correspond to a range of only 0.08 dex in [Fe/H] if one was to adopt the pseqw's without adjustment, while the dispersions correspond to an error in [Fe/H] of only 0.04 dex. These statistics from three independent studies show that use of the Ca II triplet is a simple and observationally robust metallicity index.

We list in Table 2 the adopted abundances, reddenings, and horizontal-branch magnitudes (V_{HB}) for the Galactic globular clusters and Sextans (the abundance parameter W' is defined in § 4.1). The [Fe/H] values are from the compilation in Armandroff (1989) and Zinn & West (1984). In Table 3 we list the photometric data and the W values for the individual Galactic cluster stars based on the horizontal branch luminosity and reddening data listed in Table 2. The explanatory notes to Table 3 are on the following page. In Table 4 we list the same quantities for the stars which are radial velocity members of Sextans (see below). In Table 5 we list the stars in the Sextans field that are not radial velocity members. In Tables 4 and 5 we also list the average intensity in the continuum of the co-added spectra in units of ADU where 1 ADU = 1.2 photoelectrons.

The error in the W values for the Sextans giants in principle can be estimated from the multiple observations of the same star. We found, however, that the individual spectra were too noisy to measure a meaningful pseqw. Instead, for each star, we

TABLE 2

BASIC CLUSTER PARAMETERS

Cluster	V_{HB}[a]	$E(B-V)$[a]	[Fe/H][b]	W'(Ca) (Å)	m.e. (Å)	Notes[c]
NGC 104 (47 Tucanae)	14.06	0.04	−0.71	4.75	0.03	1
NGC 288	15.30	0.04	−1.40	3.81	0.07	1
NGC 1904 (M79)	16.20	0.01	−1.68	3.20	0.05	1
NGC 2682 (M67)	10.57	0.06	−0.06	5.76	0.18	1
NGC 4590 (M68)	15.60	0.03	−2.09	1.60	0.03	
NGC 5904 (M5)	15.15	0.03	−1.40	3.89	0.03	
NGC 5927	16.70	0.45	−0.31	5.08	0.15	2
NGC 6121 (M4)	13.35	0.40	−1.33	4.08	0.04	
NGC 6171 (M107)	15.63	0.31	−0.99	4.22	0.03	
NGC 6218 (M12)	14.90	0.17	−1.61	3.90	0.06	
NGC 6397	12.90	0.18	−1.91	2.30	0.03	
NGC 6712	16.11	0.48	−1.01	4.30	0.11	
NGC 6705 (M11)	...	0.42	0.0	...	...	3
NGC 6752	13.75	0.04	−1.54	3.50	0.04	
NGC 6838 (M71)	14.41	0.27	−0.58	4.83	0.06	
NGC 7099 (M30)	15.11	0.06	−2.13	1.90	0.03	4
NGC 1851	16.05	0.02	−1.16	4.57	0.05	5, 6
NGC 6205 (M13)	14.95	0.02	−1.65	3.35	0.10	7
NGC 6341 (M92)	15.05	0.02	−2.24	1.76	0.11	7
NGC 7078 (M15)	15.86	0.10	−2.17	1.55	0.04	5
NGC 7089 (M2)	16.05	0.02	−1.58	3.42	0.03	5
Sextans dSph	20.35	0.02	−2.05	...	...	8

[a] Globular cluster horizontal-branch luminosities and reddenings from Armandroff 1989.

[b] Globular cluster [Fe/H] values from Zinn & West 1984 and Armandroff 1989.

[c] NOTES.—(1) Data discussed in Suntzeff et al. 1992. See Appendix. (2) Mean value of W'(Ca) for two faintest stars is 5.63 ± 0.07. (3) $(m - M)_{app} = 12.5$. The distance modulus, reddening, and metallicity discussed in Suntzeff et al. 1992. (4) W' for M30 data given in Appendix is 1.84 ± 0.04 Å. (5) Data from Armandroff & Da Costa 1991. (6) Metallicity from Da Costa & Armandroff (1990) and AD2. (7) Data from Armandroff, Da Costa, & Zinn 1992. (8) Horizontal-branch luminosity and reddening from Mateo et al. 1991a. [Fe/H] from this paper.

TABLE 3

PHOTOMETRY, CALCIUM II EQUIVALENT WIDTHS, AND RADIAL VELOCITIES FOR CLUSTER STARS

Star	$V - V_{HB}$	$(B-V)_0$	W (Å)	v_r (km s^{-1})	Notes
			NGC 4590 (M68)		
Q	−2.03	0.95	2.98	−91.8	
II-28	−1.88	0.93	2.94	−95.6	
I-74	−1.01	0.81	2.25	−88.5	
I-49	−0.98	0.59	2.03	−89.3	1
I-10	−2.29	1.03	2.92	−89.9	
I-2	−0.65	0.78	2.06	−90.5	
ZNG 2	−3.11	1.12	3.44	−89.3	2
I-260	−3.08	1.25	3.57	−85.6	
L	−2.70	1.09	5.45	−5.5	3
I-258	−1.36	0.83	2.40	−84.3	
I-256	−2.96	1.31	3.37	−90.4	
I-239	−1.41	0.84	2.29	−79.2	
II-79	−1.21	0.81	4.82	11.8	3
I-184	−0.55	0.89	4.64	−33.0	3
II-72	−0.57	0.82	2.22	−82.7	4
I-144	−2.80	1.26	3.43	−93.6	
I-119	−1.98	0.93	2.83	−90.0	
II-47	−0.57	0.82	2.44	−88.0	
			NGC 5927		
M873	−0.29	1.16	5.74	−112.8	
M468	−0.38	1.06	5.93	−106.0	6
M040	−1.11	1.17	5.64	−105.2	
M073	−1.55	1.46	5.89	−98.7	
V6	−0.88	1.17	4.10	−105.4	7,8
M084	−1.31	1.27	5.66	−101.0	
FG1021	−1.50	–	5.65	−111.3	
A	−0.98	–	5.65	−4.8	3
M799	−1.90	1.77	4.60	−107.4	7
M857	−1.10	1.29	5.53	−111.9	
			NGC 6121 (M4)		
1412,V4	−2.97	1.23	4.44	73.0	1,8
1514	−2.59	1.44	5.95	80.0	
1411,A219	−2.27	1.35	5.53	68.2	2
1408,B	−1.53	1.01	4.62	76.0	6
1403,C	−1.22	1.06	4.95	74.7	
1501,A243	−1.65	1.13	5.14	71.3	
2519,A423	−1.53	1.06	4.81	68.6	
2617,A529	−1.53	1.20	4.95	64.3	
2206	−1.45	1.11	4.96	69.7	
2608,A442	−1.10	1.04	4.83	80.6	
2406,V13	−2.51	1.29	4.88	73.4	1,8
3419,A308	−0.28	0.91	4.29	77.7	
3624,A459	−1.57	1.16	5.05	69.8	
3209	−2.41	1.26	5.60	63.8	1
3413,A95	−2.02	1.12	5.11	68.0	1
3612,A468	−1.53	1.07	4.96	75.7	
3701,A549	−1.17	0.99	4.44	72.9	5
4421	−0.68	0.96	4.49	67.2	
4511	−1.73	1.19	5.22	66.4	
4201	−1.64	0.98	4.68	77.9	2
4613,A516	−2.50	1.47	5.72	68.4	
			NGC 5904 (M5)		
III-78	−2.55	1.36	5.65	50.6	
Zh321	−2.26	–	5.36	48.0	
III-50	−2.27	1.10	4.92	43.8	1
III-36	−2.39	1.30	5.28	54.9	
III-18	−1.85	0.97	4.62	50.2	1
III-3	−2.78	1.47	5.71	52.3	
II-9	−2.82	1.50	5.48	60.7	
Zh191	−2.88	–	5.77	53.3	
II-50	−1.26	0.99	4.78	47.5	
Zh274	−2.18	–	5.11	58.7	
II-85	−2.86	1.56	5.81	56.4	
I-4	−1.75	1.10	4.93	62.0	
I-58	−1.86	1.12	4.96	49.8	
I-68	−2.73	1.52	5.65	60.3	
I-71	−2.05	1.17	5.01	61.5	
I-20	−2.65	1.41	4.95	53.8	5
I-25	−1.53	1.06	4.72	62.0	
I-80	−1.17	1.00	4.65	50.2	
IV-59	−2.52	1.31	5.05	59.2	2,5
IV-47	−2.77	1.47	5.51	56.9	
IV-34	−2.09	1.17	5.11	49.9	
IV-30	−1.63	0.90	4.60	52.9	1
IV-19	−2.56	1.38	5.56	44.3	
			NGC 6712		
A51	−1.84	1.28	5.56	−105.4	
KC501	−1.15	1.03	5.14	−107.4	
KC5	−1.65	1.15	5.05	−104.2	
B112	−1.54	0.91	4.85	−110.8	2
D7	−2.0	–	5.35	−111.0	
LM6	−1.43	0.99	5.15	−102.2	2
B8	−1.91	1.26	5.45	−111.2	
A6	−1.74	0.80	5.64	28.1	3
KC729	−1.15	1.04	5.67	−37.1	3
D1	−1.7	–	5.74	−106.7	
V15	−2.23	1.67	5.03	−114.3	7
I	−1.71	0.94	5.41	80.2	3
D2	−2.0	–	5.02	−101.6	
A38	−1.25	1.12	5.49	−101.1	
			NGC 6171 (M107)		
224	−1.63	0.99	4.65	−31.0	1
23	−0.89	1.07	4.56	−30.6	
16	−1.34	1.12	5.12	−32.3	2
278	−1.49	1.17	5.10	−29.8	
F	−2.24	1.39	5.65	−36.1	
273	−2.40	1.50	5.80	−28.7	
J	−1.66	1.27	5.18	−26.6	
T	−0.71	0.95	4.60	−32.8	
U	−0.85	0.97	4.61	−37.9	
H	−1.79	1.30	5.31	−29.9	
259	−0.99	0.99	4.86	−32.6	2
217	−2.74	1.63	6.00	−36.6	
201	−1.19	0.96	4.57	−28.7	2
172	−1.79	1.24	5.20	−32.6	9,22
133	−0.48	0.94	4.64	−29.2	
90	−1.26	0.70	5.14	−31.1	1,6,1
127	−1.58	1.17	5.04	−30.7	
115	−0.62	0.91	4.43	28.6	3,11
110	−1.10	0.93	4.86	−28.9	2,10
N	−1.37	1.22	5.07	−35.1	
G	−2.13	1.35	5.68	−32.4	
72	−0.97	1.08	5.13	−33.0	
62	−1.66	1.31	5.32	−32.2	

TABLE 3—*Continued*

Star	$V - V_{HB}$	$(B-V)_0$	W (Å)	v_r (km s^{-1})	Notes
		NGC 6218 (M12)			
I-2-65	−1.53	0.90	4.89	−42.6	
I-1-2	−2.61	1.19	5.74	−41.4	
I-4-15	−1.95	0.85	4.72	−38.4	
I-4-12	−2.85	1.42	5.72	−43.9	
I-3-6	−2.39	1.15	5.46	−42.8	
IV-2-63	−1.20	0.95	4.74	−35.3	
IV-1-24	−2.38	1.09	4.59	−42.8	5
5523	−2.19	0.70	5.69	−46.8	2,6,12
IV-2-10	−2.63	1.31	5.50	−41.1	
5531	−2.09	0.70	5.64	−39.8	2,6,12
III-1-3	−0.80	0.83	4.55	−36.3	
g	−2.68	1.40	5.59	−35.8	13
III-3-23	−1.16	0.94	5.17	−56.5	
III-1-28	−1.01	0.91	4.52	−45.4	
1	−3.20	0.76	5.72	−43.8	14
II-1-7	−1.93	0.99	5.21	−43.9	
668	−1.79	0.75	4.56	−42.7	
II-2-47	−1.94	0.93	5.23	−38.4	
2(5511)	−2.97	1.33	5.44	−48.2	
6512	−1.73	0.77	4.86	−39.2	
		NGC 6705 (M11)			
1184	−0.36	1.09	6.97	32.2	
1423	−0.22	1.18	7.11	36.3	
1256	−0.05	1.30	6.98	36.0	
1625	0.03	1.29	6.87	31.7	
2000	−0.16	1.11	6.98	36.4	
1837	0.28	1.07	6.16	37.3	
1446	−0.01	1.18	6.26	35.5	
1658	−0.02	1.02	6.50	33.7	
1364	0.20	0.77	5.89	32.7	
1286	0.19	0.98	6.14	33.6	
963	0.11	1.04	6.85	32.9	
779	−0.23	1.32	6.96	32.2	
827	−0.47	1.37	6.76	35.5	
411	−0.09	1.20	6.84	32.4	
686	0.25	1.04	6.58	35.9	
160	−0.06	–	6.64	33.3	
916	−0.16	1.08	6.71	33.3	
136	0.21	1.10	6.68	32.2	
669	0.28	1.17	6.90	34.2	15
1101	0.45	1.02	6.04	34.7	
1090	0.22	1.13	6.66	33.7	
320	0.12	0.98	6.71	32.1	
		NGC 6838 (M71)			
S	−1.47	1.24	5.61	−23.0	
A9	−1.47	1.30	5.78	−23.6	
KC136	0.39	0.95	4.27	−25.8	
CF8	−0.67	1.17	5.09	−18.3	18
1-95,2-63	−1.11	1.02	5.05	−20.3	2
1-77	−1.76	1.46	6.26	−29.2	19
1-71	−0.87	1.17	5.28	−15.6	18
1-113	−1.98	1.53	6.33	−22.8	19
1-45	−2.05	1.49	6.11	−22.0	
1-53	−1.44	1.34	5.59	−25.3	
1-46	−2.12	1.48	6.34	−24.4	
S232	−0.97	1.18	5.26	−25.9	
A4	−2.21	1.42	6.04	−26.4	2,18
1-14	−0.64	0.99	5.06	−24.6	
1-9,2-239	−1.12	1.00	5.16	−21.6	2
1-3	−0.03	0.93	4.85	−21.1	
1-89	−0.04	0.78	4.37	−20.1	20

Star	$V - V_{HB}$	$(B-V)_0$	W (Å)	v_r (km s^{-1})	Note
		NGC 6397			
669	−2.40	1.10	3.76	24.4	
603	−2.55	1.15	3.92	26.1	
469	−2.94	1.33	4.13	21.7	2
428	−1.40	0.87	3.09	22.2	
128	−0.66	0.79	2.83	24.4	
025	−0.68	0.78	2.72	20.9	
028	−1.09	0.76	2.70	21.8	2
043	−1.96	0.94	3.30	23.5	
012	0.68	0.65	2.30	24.6	
059	0.99	0.68	2.28	18.4	
752	0.99	0.62	2.18	18.8	
075	−0.78	0.69	2.55	27.0	1
211	−2.74	1.28	4.03	24.1	
220	0.94	0.67	2.28	26.3	
229	0.89	0.63	2.33	19.6	
686	0.60	0.62	2.32	25.6	
685	−0.89	0.79	2.94	21.5	
548	0.12	0.68	2.50	21.9	
620	0.29	0.66	2.55	17.9	
616	0.28	0.66	2.33	22.1	
		NGC 6752			
CS009	−1.38	0.99	4.30	−26.9	
CL1003	−1.38	0.97	4.72	−24.0	
CS003	−2.25	1.21	4.82	−21.0	
A08	−1.72	1.08	4.54	−34.2	
CS001	−1.36	0.84	3.92	−27.8	1
A68	−1.73	1.07	4.52	−30.8	
CS107	−1.41	1.05	4.35	−29.3	
CL1089	−2.67	1.29	–	−29.8	2,16
A59	−2.85	1.55	–	−22.0	17
CL1071	−1.06	0.93	4.22	−30.0	
CL1066	−2.22	1.18	4.96	−28.7	
CS118	−1.57	1.03	4.49	−23.1	
CS119	−0.75	0.89	3.88	−24.2	
CS121	−0.28	0.81	3.74	−24.2	
CL1048	−1.53	1.06	5.50	−38.6	4
CS126	−2.45	1.26	4.48	−24.4	16
CS128	−0.02	0.81	3.57	−27.0	
CS135	−2.31	1.11	4.61	−29.7	1
A31	−2.95	1.56	–	−23.0	17
A12	−2.50	1.31	4.92	−30.0	16
CL1015	−1.87	1.13	4.54	−26.1	
		NGC 7099 (M30)			
PE91	−2.11	1.00	3.09	−173.0	
PE89	−0.27	0.68	2.48	−174.7	
PE24	−2.05	1.03	3.17	−179.4	
PE23	−2.91	1.34	3.58	−179.9	
084	−0.40	0.66	2.28	−168.3	
066	−1.16	0.90	2.68	−174.6	
PE19	−1.97	0.98	3.16	−182.1	
PE18	−2.52	1.17	3.40	−186.8	
032	−1.35	0.81	2.72	−180.9	2
PE17	−2.50	1.15	3.14	−192.1	21
PE10	−1.51	0.95	2.94	−183.7	
160	−0.82	0.68	2.35	−179.3	2
132	−0.12	0.68	2.52	−168.5	4
139	−0.52	0.68	2.39	−181.1	
PE04	−2.28	1.09	3.28	−181.1	
115	−1.79	0.88	2.83	−179.1	2

produced a pair of roughly equal intensity spectra summed from independent spectra. The mean error, estimated from each spectral pair, is listed in Table 4. This mean error is inaccurate however, since it is based on sample sizes of only two spectra per object. To estimate a more reliable "typical" mean error, we have divided the data into three magnitude intervals and used the formulae in Olszewski et al. (1991) to estimate the sample variance for the data pairs, under the assumption that all the data in each magnitude interval have the same parent population. We find that the average mean error in W for the brightest giants in Sextans ($V < 18.0$) is $0.16^{+0.07}_{-0.03}$ Å for 10 stars; for $18.0 < V < 18.6$, $0.24^{+0.07}_{-0.04}$ Å for 14 stars; and for $V > 18.6$, $0.46^{+0.16}_{-0.08}$ Å for 11 stars. The errors in the estimated mean error were derived by setting the confidence interval in χ^2 distribution (eq. [3] in Olszewski et al.) to the 68% level which is the equivalent of a 1 σ distribution. We have also excluded a few stars from the statistics that had clearly larger mean errors than the rest of the sample (stars 12, 44, and 58). These estimates are close to the median error in each magnitude bin, namely 0.17, 0.25, and 0.43 Å.

Examples of the spectral data are shown in Figure 3, where we have plotted two members of Sextans (based on the radial velocities discussed below) compared to cluster giants All these giants have $V - V_{HB} \sim -3$. Note that the line strengths of the Sextans giants are more similar to M68 than M5, implying that Sextans must be a metal-poor object near [Fe/H] = −2. Also note that the two giants in Sextans clearly have different line strengths, indicating that this galaxy must also have a range in stellar abundances.

2.5. *Measurement of the Radial Velocities*

The radial velocities for all program and standard stars were measured with the IRAF program "FXCOR." This program performs a cross-correlation between object and template, which have been rebinned from a linear wavelength scale into units of the logarithm (base 10) of wavelength, maintaining the original number of pixels. These rebinned data are brought to a continuum level of zero by subtracting a fourth-order cubic spline fit to the data. In addition, the object spectrum was filtered in Fourier space with a simple ramp function, following the precepts of Tonry & Davis (1979). According to Tonry & Davis, the cutoff frequency at which the spectra are smoothed without substantially reducing the spectral resolution is $f_c = 1/(2\pi\sigma_{res})$, where σ_{res} is equal to (FWHM)/2.35 and FWHM is the full width at half-maximum resolution of the input spectrum. The corresponding cutoff wavenumber is $N * f$, where N here is the number of pixels used in the Fourier transform, which is the smallest value of $N = 2^n$ which is larger than the number of pixels in the original spectrum. We have found that the best cutoff wavenumber is about a factor of 2 higher than this value.

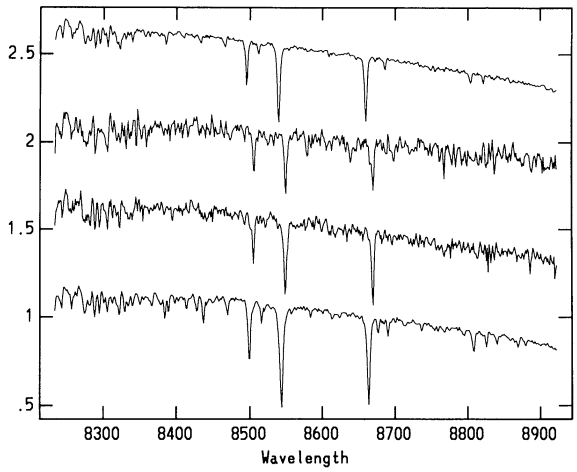

FIG. 3.—A comparison of two radial velocity members in Sextans with globular cluster giants at $V - V_{HB} = -3$. The spectra from top to bottom are M68 I-260, Sextans 49, 17, and M5 191. All the spectra have been scaled to unit intensity and shifted by units of 0.5. Note that two Sextans giants are both weak lined like M68 and yet show substantial differences in relative line strengths, implying a real star-to-star abundance variation in this galaxy.

In particular, the spectral data, which all have 570 pixels with 1.21 Å pixel^{-1} and a starting wavelength of 8234 Å, are rebinned to a 570 pixels of $\log_{10}$ wavelength where 1 pixel equals 6.1293×10^{-5} [in units of $\log_{10}$ (Å)] or 42.3 km s^{-1} pixel^{-1}. These data are continuum subtracted. The filter for the object spectrum will have a cutoff wavenumber of ~350 for a resolution of 2.3 pixels. For the actual filter, we have used a ramp where the filter is zero outside of 25 and 375 wavenumbers, and ramps linearly up to 1.0 at wavenumbers 35 and 333. The lower end of the filter is not critical since the data have already been flattened. Experiments on real data showed that

NOTES TO TABLE 3

NOTES ON CLUSTERS, PERTAINING TO SOURCES OF PHOTOMETRY AND STAR NAMES.—M68: Harris 1975. M5: Cudworth 1979. Pseqw's and velocities averaged from two frames. NGC 5927: Star numbers: M, Menzies 1974; variable V6 is identified in Menzies 1974; FG, Friel & Geisler 1991; star A is 7″ at PA = 80° from star LM1 (See Plate 1 in Lloyd Evans & Menzies 1977). V photometry average of Menzies 1974, Lloyd Evans & Menzies 1977, and Friel & Geisler (1991) (converted from $T1$). $B-V$ photometry is from Menzies 1974. The photometry for star A is $T1 = 15.02$ and $(T1 - T2) = 0.73$ (D. Geisler, private communication). M4: Cudworth & Rees 1990. Pseqw averaged from two frames. Velocities taken from long-exposure frame, except where obviously saturated. NGC 6171: Cudworth, Smetanka, & Majewski 1992 and Dickens & Rolland 1972. M12: Racine 1971 and Nassau & Hynek 1942. Racine work quotes only the photoelectric standards, and the Nassau & Hynek work is photographic photometry. Original Racine photographic photometry and the conversion of Nassau & Hynek photometry to BV provided by T. Pryor. NGC 6397: Woolley et al. 1961 and Cannon 1974. NGC 6712: Cudworth 1988. The stars marked "D" are from C. Bailyn (private communication) and are identified as D1: ~5″ NE of A15; D2: ~12″ NE of V5; D7: ~10″ NW of circular asterism of stars A70–A74. M11: Mathieu et al. 1986. Cluster has no horizontal branch due to young age. Red giant clump stars at $V \sim 11.6$. NGC 6752: Norris et al. 1981. CL numbers are from an unpublished finding chart from Cannon & Lee. M71: Cudworth 1985. Velocity variables noted from Pryor. M30: Dickens 1972.

NUMBERED NOTES PERTAINING TO INDIVIDUAL STARS.—(1) Asymptotic giant branch star. (2) Possible asymptotic giant branch star. (3) Radial velocity nonmember. (4) Velocity differs significantly from cluster mean. (5) Line strength inconsistent with color; spectrophotometric magnitude consistent with V, however. (6) Spectrophotometric magnitude inconsistent with V. Possible misidentification or star not on fiber? (7) Strong TiO. (8) Photometric variable. (9) Possible misidentification. (10) Proper motion nonmember. (11) Probable proper motion nonmember. (12) Photometry quite uncertain. (13) Spectroscopic magnitude somewhat inconsistent with V. (14) Line strength inconsistent with color. (15) Spectrophotometric magnitude inconsistent with V. Star probably not centered on fiber. (16) Spectrum near saturation on CCD. (17) Spectrum at CCD saturation. (18) Possible velocity variable. (19) Weak TiO? (20) Red horizontal branch star. (21) Cosmic-ray hit may have affected velocity measurement. (22) Star 172 not on any finding charts. Spectrophotometric magnitude of Star 172 is consistent with identification.

TABLE 4

CALCIUM II EQUIVALENT WIDTHS, STELLAR METALLICITIES, AND RADIAL VELOCITIES FOR SEXTANS GIANTS

Star	$V - V_{HB}$	$(B-V)_0$	W (Å)	m.e. (Å)	$\delta(B-V)$	[Fe/H]	v_r (km s^{-1})	$\sigma(v_r)$ (km s^{-1})	N	Intensity (ADU)	Notes
2	−1.63	1.01	2.48	0.72	0.10	−2.22	211.5	8.4	5	361	
3	−1.33	0.97	–	–	0.12	–	200.1	24.0	2	187	1
5	−2.11	1.10	2.59	0.30	0.08	−2.28	229.4	4.1	3	1108	
7	−1.71	0.74	4.54	0.53	−0.18	−1.57	209.8	7.5	3	198	2
8	−2.27	1.19	3.36	0.49	0.12	−2.06	221.8	10.4	4	853	
11	−2.18	1.11	3.08	0.13	0.07	−2.13	224.6	4.4	4	1304	3
12	−2.61	1.27	3.65	0.27	0.10	−2.04	232.0	5.9	3	632	
14	−1.83	1.08	3.16	0.25	0.12	−2.04	233.5	5.8	5	417	4
15	−1.62	0.78	3.37	0.36	−0.13	−1.93	203.4	12.0	3	325	2,5
17	−2.76	1.34	3.90	0.14	0.12	−1.99	214.6	3.4	5	2641	6
18	−2.40	1.13	3.49	0.18	0.02	−2.05	211.2	7.1	4	437	
19	−2.35	1.11	3.18	0.28	0.01	−2.14	237.6	11.5	2	433	
20	−2.94	1.98	4.00	0.25	–	−1.99	228.2	2.0	3	1509	7
22	−1.86	0.99	3.70	0.37	0.03	−1.87	201.9	12.7	3	366	5
23	−1.64	0.96	3.47	0.49	0.05	−1.90	219.0	9.5	4	279	
24	−1.63	0.93	3.31	0.33	0.02	−1.95	244.8	15.0	2	259	
25	−1.93	1.03	1.98	0.32	0.05	−2.44	235.3	9.8	3	1414	
26	−1.69	0.91	3.13	–	−0.01	−2.02	219.5	12.5	2	239	1,5
29	−1.61	1.08	4.06	0.35	0.18	−1.71	247.1	12.1	3	621	
31	−2.87	1.28	3.92	0.11	0.02	−2.00	226.5	4.9	5	2149	
32	−1.61	0.86	3.09	0.70	−0.04	−2.02	235.3	3.8	3	557	
34	−2.35	1.06	2.80	0.14	−0.04	−2.26	244.7	6.7	3	597	
35	−3.05	1.39	3.94	0.11	0.06	−2.03	219.0	5.7	3	1071	
36	−2.39	1.07	3.43	0.17	−0.03	−2.06	236.3	4.6	6	1336	
37	−1.90	0.94	2.42	0.26	−0.03	−2.29	228.2	8.5	5	394	
38	−1.45	0.85	1.88	0.40	−0.02	−2.37	221.2	6.7	3	363	
39	−1.58	0.98	3.28	–	0.09	−1.95	191.0	13.3	5	326	1,5
40	−1.98	1.07	2.97	0.20	0.08	−2.13	220.3	5.4	4	950	
41	−1.62	1.06	3.65	0.20	0.16	−1.84	202.5	12.9	4	480	5
44	−2.13	1.03	3.72	0.65	0.00	−1.92	242.4	5.3	4	967	
45	−1.58	1.03	2.78	0.43	0.13	−2.11	226.7	12.9	3	435	4
49	−2.76	1.13	2.22	0.23	−0.09	−2.52	240.3	3.3	6	2023	
50	−1.52	0.85	3.30	–	−0.03	−1.93	250.0	8.7	3	327	1,8
51	−2.50	1.24	3.89	0.23	0.10	−1.94	228.4	3.0	3	663	
52	−1.85	0.99	3.72	0.14	0.03	−1.86	222.7	2.4	4	1285	
54	−2.84	1.27	3.02	0.13	0.02	−2.28	237.8	5.7	2	556	
56	−2.98	1.41	5.05	0.07	0.11	−1.66	228.7	7.4	3	1028	
58	−2.66	1.15	4.41	0.36	−0.03	−1.80	214.5	3.6	6	1596	6
61	−2.33	1.08	2.52	0.09	−0.01	−2.34	232.1	5.3	4	1662	
71	−2.80	1.28	4.24	0.18	0.04	−1.89	231.0	7.1	5	2289	
72	−1.97	0.95	2.84	0.13	−0.07	−2.17	239.9	5.4	4	1322	4
73	−2.10	0.95	3.59	0.07	−0.07	−1.95	225.7	4.6	3	889	
76	−1.59	0.77	2.45	0.53	−0.13	−2.22	252.1	17.0	2	347	2

NOTES.—(1) Mean error in W impossible to estimate due to poor quality of spectral pairs. (2) Possible AGB star. (3) Same star observed twice by mistake. Data reduced separately, and tabulated values are averages of the two values. Velocities agreed to 2.5 km s^{-1} and W to 0.3 Å. (4) Summed spectra give significantly different W values than spectral pair. (5) Very poor correlation. Velocity estimated from mean of individual spectra much different from the velocity estimated from mean spectrum. (6) Velocity significantly different from mean galaxian velocity. (7) Very red colors. [Fe/H] very far off calibrated region. Spectrum shows Hα in emission. (8) Velocity uncertain due to cosmic ray hit near line.

the velocity accuracy substantially improved on low S/N data when the filter was used. The data are then cross-correlated over the wavelength region 8400–8700 Å, and the cross-correlation peak is fitted with the "CENTER1D" algorithm in IRAF. The cross-correlation peak was ~8 pixels FWHM and 20 pixels at full width zero intensity. Experimentation with the peak-fitting routine showed that the "width" parameter for the CENTER1D algorithm must be greater than 7, and that 11 to 15 pixels gave a stable fit. The velocity was then corrected for the heliocentric motion and the observed velocity of the template.

All the spectra were correlated against four spectra of M11 (stars 827, 916, 1364, and 1837) which were observed on the first night. The velocities for these template stars were taken from Mathieu et al. (1986). The four separate velocities were averaged together to form a single velocity per star. The spectra of the twilight sky (observed nightly) were also correlated. From the twilight spectra, it was discovered that there were small zero-point corrections to the velocity that varied from fiber to fiber but were extremely constant for each fiber during the whole run. These corrections did not exceed 5 km s^{-1} and were stable to 0.5 km s^{-1} for the whole run. Such a correction is not unexpected since we were able to linearize the data in wavelength only with low-order polynomials due to a

TABLE 5

RADIAL VELOCITIES OF FIELD STARS TOWARD SEXTANS

Star	v_r (km s^{-1})	Intensity (ADU)
1.....	27.2	2502
4.....	21.4	2353
6.....	10.4	361
9.....	26.0	1499
10.....	9.9	2808
13.....	8.1	2235
16.....	35.8	686
21.....	34.8	4701
27.....	91.8	558
28.....	23.9	2449
30.....	55.8	1051
33.....	33.7	9738
42.....	−34.2	733
43.....	43.5	1388
46.....	6.0	2938
47.....	−18.6	2591
48.....	7.4	3882
53.....	−4.4	1601
55.....	1.2	4509
57.....	2.5	360
59.....	11.6	1917
60.....	6.8	4874
62.....	−12.3	1737
63.....	123.0	1569
64.....	−13.6	2843
65.....	−12.6	1828
66.....	−41.4	786
67.....	14.6	739
68.....	12.5	316
69.....	2.3	3663
70.....	−14.4	2144
74.....	19.2	4559
77.....	49.2	5595
78.....	−36.2	697
79.....	41.4	623
80.....	243.2[a]	271
81.....	68.4	530

[a] Star 80 velocity suggests possible Sextans membership, but correlation too poor for reliable velocity.

limited number of lines in the helium-argon arc. The fact that the fiber-to-fiber zero-point corrections varied continuously as a function of fiber number is consistent with the fact that the higher order terms in the optical distortions in the spectrograph were not removed in the wavelength calibration.

The final velocities are listed in Table 3 for the cluster stars, and in Tables 4 and 5 for the stars in the Sextans field. For the stars in the Sextans field, we have used the co-added spectra as the object spectra. However, in order to estimate the velocity accuracy for the stars which are members of the Sextans galaxy, we have also correlated the *individual* spectra and calculated an error in the mean. For a given star, all the correlations of the individual spectra were examined and a weight assigned by hand according to the height of the cross-correlation peak. Occasionally, when visual inspection of the spectra showed what might be poorly subtracted night-sky lines, the wavelength interval for the correlation was adjusted slightly, usually to exclude the line at λ8496. Without this adjustment, the velocity occasionally differed by more than 40 km s^{-1} from the mean. The weighted mean errors (weighted by the scheme described below) and the number of spectra used in the calculation of the mean errors are listed in Table 4.

In Table 6 we list the mean cluster velocities based on the data in Table 3, the *observed* velocity dispersions (uncorrected for observational errors), and the number of cluster members used in the means.

2.6. *Accuracy of the Radial Velocities*

The velocity accuracy of the data can be divided into three parts: the error in the fiber-to-fiber velocity zero point, the error in the zero point of the whole velocity system with respect to velocity standards, and the error in single measurements of the program stars. The latter error has already been discussed and appears in Table 4.

The accuracy in the fiber-to-fiber velocities is no better than the dispersion in the nightly spectra of the twilight skies. In Table 7, we list the nightly standard deviation in the velocities of the twilight sky measured through the 23 fibers, where it can be seen that the dispersion was 0.6 km s^{-1} or better. As an independent check, we can measure the dispersion of the stellar velocities against measurements by other groups who have obtained velocities of higher accuracy for the same stars. These comparisons are also listed in Table 7. For M11, our three measurements differ from the velocities published by Mathieu et al. (1986) with an estimated standard deviation of 1.4 km s^{-1} or less. If we average the velocities for the 17 stars observed on all three nights, the dispersion in the difference between our measurements and the published measurements is only 1.0 km s^{-1}, which must represent an upper limit to the dispersion in the fiber-to-fiber errors. Evidently, each fiber is on the same velocity system to better than 1.0 km s^{-1}, and is probably as good as 0.6 km s^{-1}.

The accuracy of the zero point of the whole velocity system can also be judged from the data in Table 7. Relative to the Mathieu et al. (1986) work, our velocities are 0.4 km s^{-1} *smaller*, and relative to the globular cluster velocities measured by three different groups, our velocities are 1.1 km s^{-1} *larger*. Since it is not clear which velocity system is correct, we have decided not to shift our velocity system to one or the other zero points. We conclude that the average velocity zero point is determined to 1 km s^{-1}.

During the night, we obtained comparison spectra roughly once an hour. From this data, we find that the average drift is 0.01 pixel h^{-1} or 0.4 km s^{-1} h^{-1}. There were also a few cases

TABLE 6

MEAN VELOCITIES AND OBSERVED VELOCITY DISPERSIONS FOR THE CLUSTERS

Cluster	v_r (km s^{-1})	$\sigma(v_r)$[a] (km s^{-1})	Number of Stars
NGC 4590 (M68)	−88.6	4.2	15
NGC 5904 (M5)	53.9	5.6	23
NGC 5927	−106.6	4.8	9
NGC 6121 (M4)	72.4	4.6	14
NGC 6171	−31.8	2.8	22
NGC 6218 (M12)	−42.6	5.1	20
NGC 6397	21.9	3.1	17
NGC 6712	−106.9	4.5	11
NGC 6705 (M11)	34.0	1.7	22
NGC 6752	−27.3	3.4	18
NGC 6838 (M71)	−23.5	2.5	14
NGC 7099 (M30)	−178.2	5.3	15

[a] Tabulated values for $\sigma(v_r)$ represent the dispersion calculated directly from the measured velocities and are uncorrected for observational error.

TABLE 7

COMPARISON OF CLUSTER VELOCITIES WITH OTHER SOURCES

Cluster	$\Delta(v_r)$[a] (km s^{-1})	$\sigma(v_r)$ (km s^{-1})	Number of Stars	Notes[b]
Night 1:				
M4	1.2	1.3	14	1
NGC 6712	1.2	1.5	7	2
M11	−0.4	1.4	21	3
Twilight	...	0.5	23	...
Night 2:				
NGC 6171	1.1	1.9	23	4
M11	−0.4	1.0	21	3
Twilight	...	0.6	23	...
Night 3:				
M12	0.9	1.4	20	4
M71	0.7	1.9	14	4, 5
M11	−0.3	1.4	18	3
Twilight	...	0.6	23	...
M11	−0.4	1.1	17	3, 6

[a] $\Delta(v_r)$ given as the average difference of our measurements *minus* the published values.

[b] NOTES.—(1) Only high S/N data used in averages. M4 velocities from Peterson, Cudworth, & Rees 1993. (2) Velocities from Charles Bailyn (private communication). (3) Velocities from Mathieu et al. 1986. (4) Velocities from Tad Pryor (private communication). (5) Excludes known velocity variables. (6) Average of the 17 stars observed in common on all three nights.

when the spectra shifted suddenly, by 0.04 pixel or 1.7 km s^{-1}. Since the wavelength solution is interpolated in time, all pixel shifts should be taken out to roughly half these values, or less than 1 km s^{-1}.

Five stars were observed in common with the Da Costa et al. (1991) study. The mean difference (in the sense of this study minus Da Costa et al.) is −7.7 km s^{-1} with a dispersion of 23 km s^{-1}. They state the average uncertainty as "on the order of 20 km s^{-1}" which is consistent with the statistics here, although the tabulated uncertainties for these five stars are closer to 15 km s^{-1}, indicating a probable underestimate for the true errors in their study.

3. THE VELOCITY DISPERSION OF SEXTANS

A histogram of the velocities of the stars in the Sextans field shows two peaks, one near 12 km s^{-1} and the other at 228 km s^{-1}. The former are obviously Galactic field stars in the direction of Sextans, and we have listed them in Table 5. The latter group of stars, which are listed in Table 4, must be members of the Sextans dwarf galaxy, and have the same velocity as reported by Da Costa et al. (1991) for six giants in Sextans.

We have calculated the mean velocity and intrinsic velocity dispersion for the Sextans giants from the formulae given in Armandroff & Da Costa (1986, hereafter AD1). These formulae are weighted sums, where the weights are the inverse square of the velocity uncertainties listed in Table 4. The error in the velocity dispersion was calculated from the formulae for the estimated error in the intrinsic velocity variance as described in AD1. To calculate the error in the dispersion from the error in the variance, we note that if μ is the intrinsic variance and $\sigma_{\rm int}$ is the intrinsic velocity dispersion where $\mu = (\sigma_{\rm int})^2$, then

$$\epsilon(\sigma_{\rm int}) = \epsilon(\mu)/(2\sigma_{\rm int}) ,$$

where ϵ refers to the error in the quantity.

Some care must be used in applying the formulae given in AD1. The procedure of estimating the intrinsic velocity dispersion from the observed dispersion was discussed initially by Trumpler & Weaver (1953) in the simpler case where all the weights are the same. AD1 have introduced the important concept of a *weighted* velocity dispersion, which allows data of unequal weights, such as those in Table 4, to be used to calculate the intrinsic velocity dispersion from the observed velocity dispersion. Their estimate for the error in the intrinsic variance, however, assumes an unweighted variance, which is inconsistent with their formula for the weighted estimate of the intrinsic variance.

This can be trivially seen from the term given for the "statistical error for the finite number of stars observed," namely

$$\epsilon_1 = \mu(2/N)^{1/2} , \quad (1)$$

where μ is the intrinsic variance, and N is the number of objects observed. The statistical error decreases as $(N)^{-1/2}$ independent of the quality of the data, whereas data of low weight do not appreciably change the estimate for the intrinsic variance. The error formulae in AD1 are actually derived in Jones (1970) for the case of the unweighted variance. The Jones (1970) formulation also assumes that the uncertainty in the mean error of velocity of each star is

$$\epsilon(\xi_i) = \xi_i/(2n_i)^{1/2} , \quad (2)$$

where ξ_i is the mean error for the ith star, and n_i is the number of observations of the ith star. We have used the same notation as equation (4) in AD. Both equations (1) and (2) are taken from Trumpler & Weaver (1953, p. 190). This formalism is only precisely valid for large N and n_i since the statistical errors are not normal distributions for small sample sizes. Interval estimates using χ^2 distributions are more accurate for these sample sizes, but since we are trying to estimate only the error in the dispersion, the small inaccuracies in the analytical formulae should not be important.

In order to avoid the preceding problems, we have chosen to estimate the velocity dispersion by breaking the sample into groups of similar velocity errors. A plot of the ξ_i as a function of continuum intensity shows a sudden increase in ξ_i below 500 ADU, which we will take as the natural dividing line between the accurate and inaccurate velocities. For the group with an "intensity" $I > 500$ ADU, we exclude the two stars with $\xi_i >$ 10 km s^{-1} which clearly have much different errors than the rest of the group, and divide the group in two halves at $\xi_i = 5.0$ km s^{-1}. In Table 8, we give the estimated velocity dispersions and their associated errors, for the whole group, and for the lower and higher accuracy halves. The means velocities listed in Table 8 are the weighted means, while the mean error has been calculated from the unweighted data. We also estimate the velocity dispersion based on the low-accuracy data ($I < 500$ ADU) for all the stars with $\xi_i < 12.5$ km s^{-1}. The final entry in Table 8 is the weighted mean of the three estimates, and the final mean error in the estimated velocity dispersion.

From Table 8, we see that the mean velocity of Sextans is 227.9 ± 1.8 km s^{-1} where we have added in quadrature the mean error and a representative error for the uncertainty in the system velocity zero point of 1 km s^{-1}. This is identical to the velocity quoted by Da Costa et al. (1991) of 230 ± 6 km s^{-1}, to within the errors.[4] In addition, we find that the velocity dispersion of Sextans is 6.2 ± 0.9 km s^{-1} based on 33 stars.

[4] Star 49 observed by Da Costa et al. (their number DC17) was listed as a nonmember, but is clearly a member based on our measurements. This star was not included in their estimate for the mean velocity.

TABLE 8

MEAN VELOCITY AND INTRINSIC VELOCITY DISPERSION FOR SEXTANS

Sample Characteristic	$\langle v_r \rangle$ (km s^{-1})	m.e. (km s^{-1})	$\sigma(v_r)$ (km s^{-1})	Error[$\sigma(v_r)$] (km s^{-1})	Number of Stars	Notes[a]
$I > 500, \xi < 10$ km s^{-1}	228.1	1.8	6.7	1.1	23	
$I > 500, \xi < 5$ km s^{-1}	226.8	2.3	6.5	1.4	12	
$I > 500, 5 < \xi < 10$ km s^{-1}	232.8	2.5	5.9	1.6	11	
$I < 500, \xi < 12.5$ km s^{-1}	221	4	6.1	2.6	10	1
Weighted average	227.9	1.5	6.2	0.9	33	2

[a] NOTES.—(1) Excludes star 50 which has very discordant velocities between two estimates. (2) Average weighted by errors.

The fact that all three independent groups of stars gives us the *same* estimated velocity dispersion gives us confidence that we are actually resolving the dispersion. We note, however, that there are two problems that lead us to be a little less confident in our final result. The first problem is that the estimated velocity dispersion of 6.2 km s^{-1} is close to the average error in a typical Sextans giant. The final estimated velocity dispersion depends critically on the accuracy of the individual velocity errors. For example, if we increase or decrease the estimated individual errors by 50%, the dispersion for the sample with $\xi_i < 10$ km s^{-1} and $I > 500$ (23 stars) will change from 6.7 km s^{-1} to 5.0 or 7.6 km s^{-1}. But we have actually measured the velocity error from individual spectra (something not often done in studies of other dwarf spheroidal galaxies) and used normal statistics to estimate the uncertainty in the velocity errors, so it is unlikely that our errors are off by such a large amount. Still, one must be very cautious about any estimated velocity dispersion when the measurement errors are roughly equal to that dispersion.

The other worry we have about the data is that the underlying distribution may not be Gaussian. In Figure 4, we plot the estimated velocity as a function of intensity in the continuum. Two stars stand out from the distribution, 17 and 58. These stars are more than 2 σ (where σ is the galaxian dispersion) from the galactic mean. The probability that one or more objects lie more than 2 σ from the mean in a sample size of $\sim$20 is 0.5, so the existence of these "outliers" is expected. However, if for the moment we exclude these two stars from the sample with $I > 500$ ADU and $\sigma < 5.0$, the estimated velocity dispersion for our "best" sample is now 4.3 $\pm$ 1.1 km s^{-1} with a weighted mean of 229.0 $\pm$ 1.8 km s^{-1}. Exclusion of these two stars also brings the means of the two samples of bright stars much closer together. These two stars could be binaries or perhaps members of a tidally disrupted group that has been suggested by Gould et al. (1992) based on the existence of an excess of subdwarfs at the distance and position of Sextans. Only more accurate and multiple epoch observations of these giants will clarify these two problems. At this stage, however, there is no statistical reason to exclude these stars from the determination of the velocity dispersion.

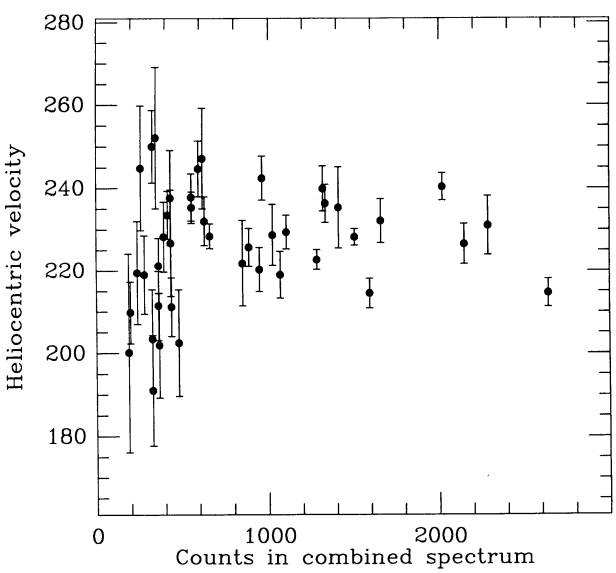

FIG. 4.—The velocities of the members of Sextans plotted as a function of intensity in the continuum. The error bars refer to the estimated mean errors of each object. The horizontal scale is in units of ADU, where 1 ADU = 1.2 electrons. Note that stars 17 and 58 lie well away from the galactic mean of 228 km s^{-1}.

4. THE METALLICITY OF SEXTANS

4.1. *Metallicity Calibrations*

To measure [Fe/H], we have adopted the technique used by AD2, ADZ, and Da Costa et al. (1992), where the summed pseqw of the two strongest members of the Ca II triplet lines, W, is plotted as a function of the brightness of the star above that of the mean horizontal branch, $V - V_{HB}$. We plot the calibration data for the clusters with excellent photometry in Figure 5.

This technique relies on the fact that the slope in the W versus $V - V_{HB}$ relation for a given cluster appears to be independent of the metallicity of the cluster. We find these same trends in Figure 5, with the following exceptions. The slope appears to change in the case of NGC 6397 for stars fainter than $V - V_{HB} \sim -0.5$. M71 has a slightly steeper slope than the rest of the globular clusters. Finally, although we did not plot the data in Figure 5, the relationships are somewhat confused at the high metallicity end. NGC 5927 lies between M11 and M71 at $V - V_{HB} \sim -1$, consistent with the metallicity of this cluster (Armandroff 1989), but lies on the M71 relation at -2. Evidently, the line strengths in the brighter giants in NGC 5927 are too weak, possibly due to blanketing effects from TiO or CN. Olszewski et al. (1991) have shown that the presence of TiO can drastically reduce the Ca II line strengths.

To calibrate W as a function of $V - V_{HB}$, we will only consider giants brighter than -0.5 in $V - V_{HB}$ listed in Table 3. We will also exclude all asymptotic giant branch (AGB) stars, stars with doubtful identifications, or stars with doubtful cluster membership as listed in the notes to Table 3. For the seven clusters shown in Figure 5 plus NGC 6171, we find the slope of the (W, $V - V_{HB}$) relationship to be -0.64 ± 0.03(m.e.). This is the same as the slope found by AD2, namely -0.62 ± 0.01. We

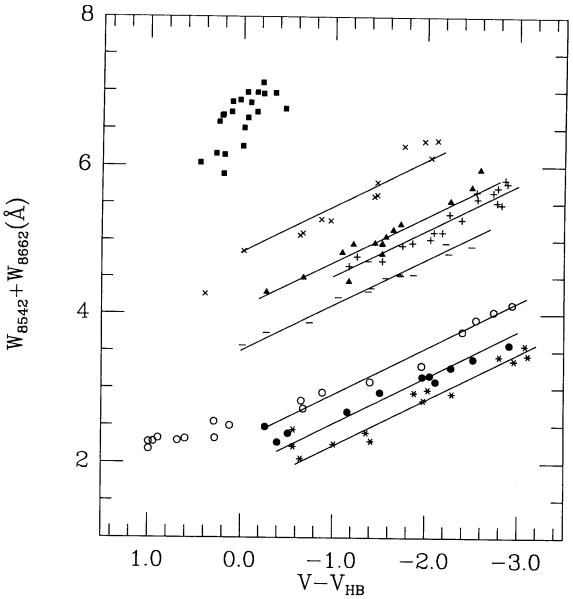

FIG. 5.—$W_{8542}+W_{8662}$ plotted as a function of $V-V_{HB}$ for the globular clusters used in the abundance calibration. The symbol definitions are (in order of decreasing metallicity) M11, *filled squares*; M71, Xs; M4, *filled triangles*; M5, *pluses*; NGC 6752, *dashes*; NGC 6397, *open circles*; M30, *filled circles*; and M68, *asterisks*. The straight lines are the best-fit ridge lines with constant slope of 0.62 (see text), fitted to the data with $V-V_{HB}<0$.

will therefore adopt the "reduced" W, or W',

$$W' = W_{8542} + W_{8662} + 0.62(V_{HB}) \quad (3)$$

as the luminosity-corrected pseqw. For each cluster, we have calculated the average W', which we list in Table 2, along with the error in the mean value.

In order to improve the metallicity calibration, we have added other clusters to the database prior to the final calibration. In the Appendix, we list W values for giants in 47 Tucanae, M79, NGC 288, and M67, measured from spectral data discussed in Suntzeff et al. (1992). These data were taken with the identical setup as used in this work. The $\langle W'\rangle$ values for these clusters are given in Table 2. M30 was also observed by Suntzeff et al. (1992). From their data, we find $\langle W'\rangle = 1.84 \pm 0.04$Å (m.e.) for 10 stars, which is the same as the value for M30 in Table 2, to within the observational errors.

We have also added the data from AD2 and ADZ to our calibration. Using the data in ADZ but our definition of W', we find for four clusters in common (M4, M5, NGC 6171, and M71), the difference in W' (in the sense of our value minus that of ADZ) is -0.29 ± 0.05 Å(m.e.). We have applied this shift, which is very similar to the difference in W of -0.25 Å based on *individual* spectra discussed above, to the ADZ data. For the AD2 data, only two clusters are in common with this work, so we have used the difference of -0.12 Å discussed above, to bring their $\langle W'\rangle$ onto our scale. We find that for NGC 6397, the AD2 value for $\langle W'\rangle$ is 2.23 Å based on eight stars, which is very close to the value 2.30 Å measured here. 47 Tucanae, however, has a value of $\langle W'\rangle = 4.95$ Å, which is significantly different than for the data in this work. This difference is most likely due to the systematic errors that arise when fitting stellar lines that are noticeably non-Gaussian with a Gaussian function. We list our recalculation of the $\langle W'\rangle$ values for clusters studied by AD2 and ADZ but not observed as part of this project, in Table 2.

In Figure 6, we plot the mean reduced W' for the 20 calibrating clusters. As can be seen, there is a very tight one-to-one correspondence between W' and [Fe/H], where the [Fe/H] values have been taken from Zinn & West (1984) and Armandroff (1989). The sudden change in slope at [Fe/H] ~ -1 has been previously noted by AD2 and ADZ. These authors have suggested that the slope change is due to the nonlinear relationship of [Ca/Fe] as a function of [Fe/H] where it is known that [Ca/Fe] goes from +0.3 dex for stars more metal-poor than [Fe/H] < -1 to [Ca/Fe] = 0 for solar-type stars (Wheeler, Sneden, & Truran 1989). A linear regression fit to the data for [Fe/H] < -1.2 yields

$$[\mathrm{Fe/H}] = -2.687 + 0.320W' \quad (4)$$

for 13 clusters. This is identical to the relationship derived by AD2, to within the errors. The dispersion in the fit was 0.08 Å. The error in a predicted metallicity based on this fit in the region of calibration is approximately $\sigma/(N-2)$ where $N = 13$, or 0.03 dex.

4.2. *The Mean Metallicity of Sextans*

In Table 9 we present the mean metallicity of Sextans based on the data for the summed pseqw's given in Table 4. The mean metallicity of Sextans is $\langle$[Fe/H]$\rangle = -2.05 \pm 0.04$ where we have added in quadrature the mean error in $\langle$[Fe/H]$\rangle$ for the samples defined in Table 9 and the estimated error of 0.03 dex in the metallicity fit. The mean metallicities have been weighted by the inverse of estimated mean errors (squared) in W for the magnitude ranges discussed above. We also list in Table 9 the estimates for $\langle$[Fe/H]$\rangle$ in the individual magnitude ranges. The mean metallicity for Sextans is the

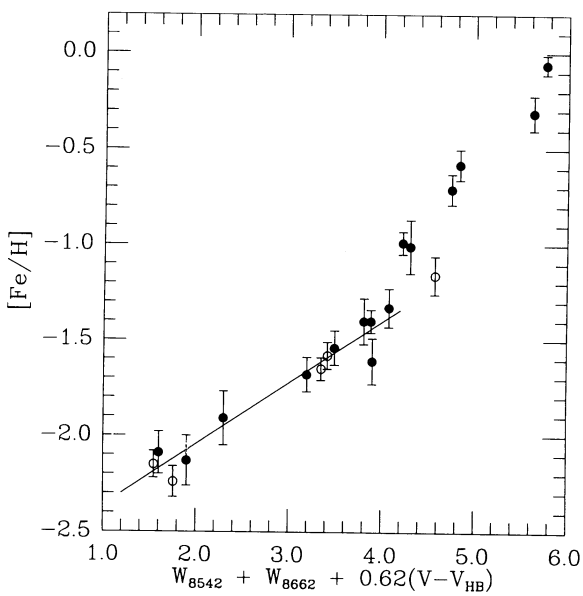

FIG. 6.—The averaged "reduced" equivalent width of the infrared Ca II lines for the calibrating clusters used in this study. The solid points refer to data presented in Table 3 or the Appendix, and the open circles to the data given by Armandroff & Da Costa (1991) and Armandroff et al. (1992). The vertical error bars are the estimated errors in the cluster abundances given by Zinn & West (1984). The errors along the abscissa are equal to or smaller than the size of the symbol. The linear regression based on the data for all the clusters with [Fe/H] < -1.2 is also shown and represents the adopted metallicity calibration. The point for NGC 5927 represents the mean value for the fainter stars (see Table 1).

TABLE 9

MEAN METALLICITY AND INTRINSIC METALLICITY DISPERSION FOR SEXTANS

Sample Characteristic	⟨[Fe/H]⟩	m.e.	σ([Fe/H])	Error (σ[Fe/H])	Number of Stars
Spectroscopic Abundances					
$V < 18.0$	−2.02	0.06	0.21	0.05	12
$18.0 < V < 18.6$	−2.13	0.05	0.16	0.03	15
$V > 18.6$	−1.99	0.07	0.18	0.05	11
All stars	−2.05	0.03	0.19	0.02	38
Photometric Abundances					
$V < 18.0$	−2.15	0.05	0.15	0.04	12
$18.0 < V < 18.6$	−2.14	0.06	0.21	0.04	15
$V > 18.6$	−1.96	0.10	0.33	0.08	12
All $V < 18.6$	−2.15	0.04	0.17	0.02	27
All stars	−2.09	0.04	...	...	39

NOTES.—For spectroscopic abundances, stars 3, 26, 39, and 50 not included due to unknown errors in W. For photometric abundances, stars 7, 15, and 76 not included due to very blue colors implying possible membership on AGB. Star 50 not included in either abundance determination due to very red color.

same for all three magnitude ranges to within the errors. Note that the typical errors in the V photometry given in Table 1 which can affect the metallicity determination through formulae (3) and (4) contribute negligibly to the errors in [Fe/H].

We can also estimate the mean metallicity of Sextans by comparing the position of the RGB of Sextans with those of Galactic globular clusters with well determined RGB photometry. In Figure 7 we plot the stars observed in the field of Sextans with the ridge lines of the globular clusters M92, M3, and 47 Tucanae published by Sandage (1982). The ridge lines have been calculated on true distance moduli calculated from the (V_{HB}, [Fe/H]) relationship used by Olszewski et al. (1991). These are slightly different than the values used by Sandage (1982) to plot the ridge lines in his Figure 6 since he used a different (V_{HB}, [Fe/H]) relationship. The assumed true distance modulus of Sextans is 19.64. We have measured the distance in $(B-V)_0$ at fixed V_0 from the M92 ridge line for all the radial velocity members of Sextans. This measure, called $\delta(B-V)$, is positive for stars redward of M92 in $(B-V)_0$. We list this quantity in Table 4.

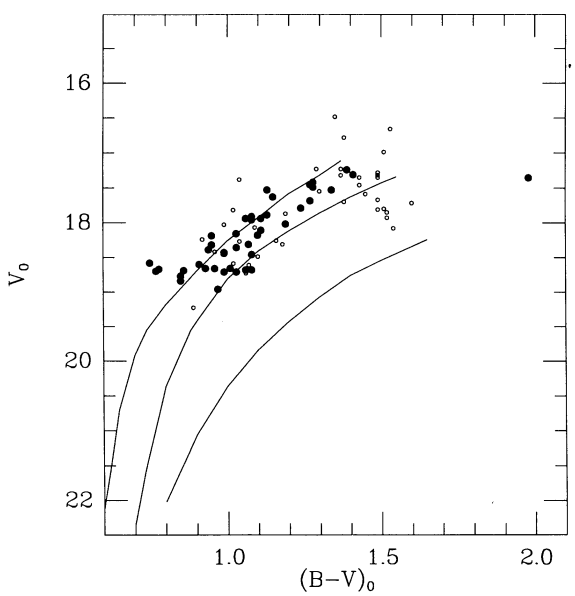

FIG. 7.—Color-magnitude diagram for the stars observed spectroscopically in the direction of Sextans. The filled circles refer to radial velocity members, and the small open circles to nonmembers. The ridge lines for the Galactic globular clusters (*left to right*: M92, M3, and 47 Tucanae) have been shifted to the distance of Sextans.

The parameter $\delta(B-V)$ cannot be converted directly into [Fe/H] since the giant branches of globular clusters tend to separate at fixed V_0 as one ascends the giant branch. Instead, we have first normalized $\delta(B-V)$ by dividing it by the factor

$$\Delta = 0.155 + 0.080M_V + 0.054M_V^2 , \quad (5)$$

which is valid for $-2.3 < M_V < -0.7$. The factor Δ is merely a measure of the separation of the M92 and M3 ridge lines given in Figure 7. The normalized $\delta(B-V)$ can now be converted to [Fe/H] using the abundances for M92 and M3 given by Zinn & West (1984). The extremely red color of star 20 precluded measurement of [Fe/H] with this technique.

The average abundance based on the $\delta(B-V)$ measures is $\langle[Fe/H]\rangle = -2.09 \pm 0.04$ for 39 stars, where we have excluded the three stars 87, 137, and 351 which lie well to the blue of the M92 ridge line, and are possibly AGB stars. We have also excluded star 20 which is too red to be calibrated. This mean has been calculated using only the photometric errors as weights. The true error must contain the photometric zero-point uncertainty (0.03 mag), the uncertainty in the abundances for the two calibrating clusters, and the errors in the distance moduli to the clusters and Sextans. The first two uncertainties contribute only about 0.07 dex each error to [Fe/H]. The dominant error is the uncertainty in the distance modulus. The error of 0.2 mag in modulus implies an uncertainty of 0.2 dex in [Fe/H], according to the formula in the following section. A more realistic photometric abundance of Sextans is therefore $\langle[Fe/H]\rangle = -2.1 \pm 0.2$.

The photometrically determined abundance confirms the abundance based on the spectra, but is different than previously published values. Mateo et al. (1991a) find $\langle[Fe/H]\rangle = -1.5 \pm 0.2$ based on photometric indicators, while Da Costa et al. (1991) find a spectroscopically determined mean abundance for Sextans of -1.7 ± 0.25. Based on the data presented here, these abundance estimates by Mateo et al. and Da

Costa et al. are somewhat too high insofar as their error estimates are correct.

4.3. *Metallicity Dispersion in Sextans*

Most of the Sextans giants have a typical mean error in W of 0.25 Å or less, corresponding to an uncertainty in [Fe/H] that is less that 0.08 dex. This is much less than the observed dispersion of $\sim$0.22 dex. The abundance dispersion in Sextans can therefore be determined to rather high accuracy. In Table 9 we list the estimated intrinsic dispersions in [Fe/H] based on the spectroscopic abundances for the various ranges in magnitude previously considered. This intrinsic dispersion and the associated error in the dispersion were calculated with the same formulae used in the velocity analysis in § 3. We have used the average mean errors and the uncertainties in these errors in W listed in § 2, to calculate the intrinsic dispersion.

Table 9 shows that the intrinsic metallicity dispersion in Sextans based on the spectroscopic abundances is 0.19 ± 0.02 dex, independent of the magnitude range of the sample.

Independent verification of this dispersion can be found in the photometric abundances. The photometric abundances are of somewhat lower quality however. Given the typical separation of the giant branches of M92 and M3 at $M_V = -1.5$ of 0.16 mag, the intrinsic dispersion in [Fe/H] corresponds to a photometric dispersion of 0.05 mag which is only slightly higher than the typical photometric error. In Table 9 we list the estimated intrinsic dispersion in [Fe/H] based on the photometric abundances for the various magnitude ranges. For the brightest sample of stars where $V < 18.6$, we find an estimated metallicity dispersion of 0.17 ± 0.02 dex, in agreement with the previous estimate.

The abundances derived for the same star using the two preceding techniques should correlated. In Figure 8, we plot the abundance estimates for the brightest group of Sextans giants ($V < 18.2$), excluding all the stars with errors in W greater than 0.2 Å as given in Table 4. One can see there is clear correlation between the two estimates of [Fe/H] supporting the existence of a real abundance dispersion in Sextans. This correlation cannot be due to simple errors in V. This is because an error in V which causes the star to appear too bright will make the star appear more metal-poor in the $(W', V - V_{HB})$ plot in Figure 5, while it will appear more metal-rich in the C-M diagram of Figure 7 (the star will move slightly brighter but much redder).

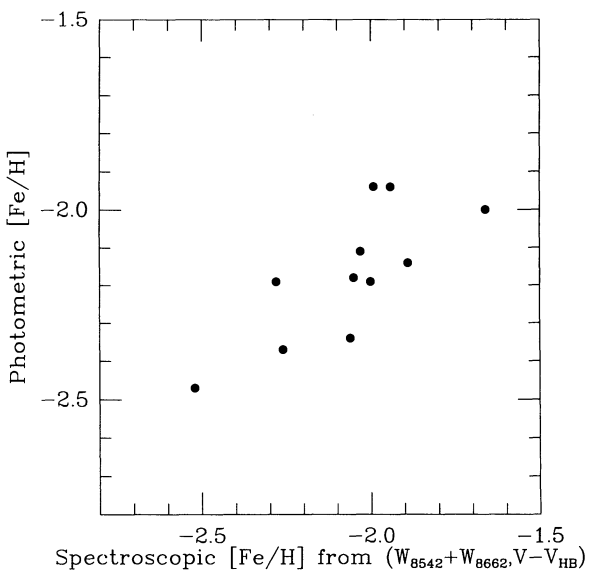

FIG. 8.—The [Fe/H] metallicity for the bright giants in Sextans determined from spectroscopy plotted against the metallicity determined from the position of the giant in the color-magnitude diagram.

Although the agreement is excellent between the two estimates for the intrinsic metallicity dispersion, caution is needed in interpreting the results. Figure 8, while showing an obviously real correlation, also displays a larger dispersion than anticipated. The mean difference been the two estimates has a dispersion of 0.15 dex, which should be compared to the quadrature sum of the typical errors for the two [Fe/H] determinations. For the spectroscopic abundances, the typical error in W is 0.16 Å or 0.05 dex in [Fe/H], while the typical error in $(B-V)$ of 0.025 for the bright giants corresponds to 0.08 dex in [Fe/H]. The total predicted dispersion based solely on the errors would be less than 0.10 dex.

It is difficult to pinpoint the source of this "extra" error. A potentially serious problem is the inclusion of AGB stars in the sample of program objects. The variation of W at fixed $(V - V_{HB})$ as a function of [Fe/H] is primarily due to both the variation in line opacity and position of the Hayashi track. That is, a metal-poor star has smaller W at fixed $(V - V_{HB})$ both because the lines are weaker (due to lower [Fe/H]) and because the star is hotter (due to the bluer Hayashi track). An AGB star, at fixed $(V - V_{HB})$ appears bluer than the red giant branch (RGB) at fixed $(V - V_{HB})$ and will therefore be measured as too metal-poor using the $\delta(B-V)$ photometric abundance estimator. Similarly, for the $(W, V - V_{HB})$ spectroscopic abundance estimator, it can be seen in Figure 5 that an AGB star will move to the right at fixed W, and also appear more-metal poor.

The effect of the AGB contamination is much larger on the photometric abundance indicator however. For stars brighter than $M_V \sim -1$, the RGB and AGB do not separate by more than about 0.25 mag (see the cluster ridge lines in Sandage 1982). For the spectroscopic technique, a star which appears 0.25 mag brighter will be measured as $0.25 \times 0.62 \times 0.32 = 0.05$ dex too metal-poor, if we ignore any gravity effects on the line strengths. For the photometric indicator, an AGB star which is brighter by ΔV will appear more metal-poor by the factor

$$\Delta V \times \left[\frac{d(V)}{d(B-V)}\right]^{-1} \times \left\{\frac{\partial(B-V)}{\partial[\mathrm{Fe/H}]}\bigg|_V\right\}^{-1}. \quad (6)$$

At $M_V = -1.5$, the slope of the RGB in M92 is $d(V)/d(B-V) = -3.5$, and the shift of the Hayashi track at fixed V as a function of [Fe/H] is 0.32. An AGB star that is only 0.2 mag brighter than the RGB will appear 0.2 dex too metal-poor. Thus the inclusion of AGB stars with modest increases in brightness could account for the larger than expected dispersion seen in Figure 8, while essentially not affecting the abundance estimated from the spectroscopic data.

In Figure 9 we plot the histogram of metallicities for the stars in the Sextans dwarf galaxy. While the number of stars is still too small to fit models, some interesting trends can be seen in the data. The histogram can be characterized as having something like an exponential tail to lower metallicities and a somewhat sharper cutoff above metallicities of [Fe/H] = −1.8. The distribution to lower metallicity is reminiscent of the exponential distribution of "G-subdwarf" metal-poor

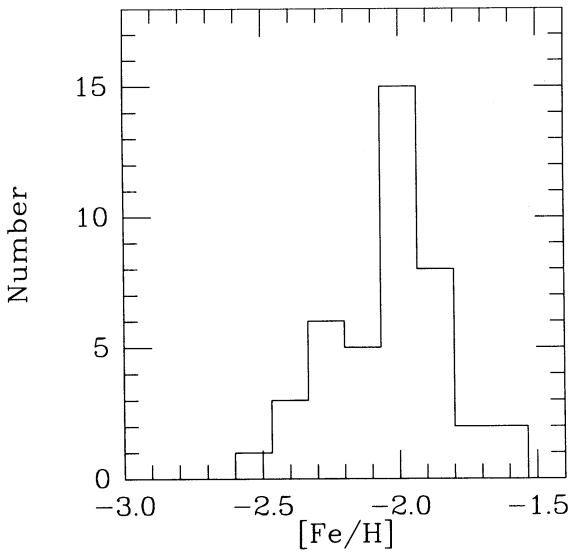

FIG. 9.—Histogram of stellar abundances in the Sextans dwarf galaxy based on the Ca II infrared triplet spectrophotometry.

field stars in the Galactic halo (van den Bergh 1962; Schmidt 1963), whose formation can be described by a simple model of isolated chemical evolution with instantaneous recycling of new metals produced in supernovae (Searle 1972): the "closed-box model." The turnover of the metallicity from the simple exponential behavior has a number of explanations, but perhaps the most reasonable is the quick removal of gas from the galaxy (Hartwick 1976). Similar metallicity distributions have been seen in other Milky Way dSph galaxies (Suntzeff 1992) and are quite distinct from the metallicity distributions in the globular clusters ω Centauri and M22 whose distributions tail off towards metal-rich stars. A much more complete census of the metallicity distribution of the Sextans giants must be obtained to verify these trends, however.

4.4. *Discussion*

Since the announcement of the preliminary results of this survey (Mateo et al. 1992a), two papers have already appeared incorporating these abundance results in the context of other dwarf elliptical systems (Da Costa 1992; Caldwell et al. 1992). Rather than repeating their discussion, we will summarize their results as follows: It is found that our determination of [Fe/H] for Sextans fits in very well with the trend of (M_V, [Fe/H]) found for the other Local Group dSph galaxies, whereas the initial measurement by both Mateo et al. (1991a) and Da Costa et al. (1991) showed that Sextans was anomalously metal-rich for its luminosity. The trend of (M_V, [Fe/H]) can be fitted by models of dwarf galaxy formation (Dekel & Silk 1986) which predict $Z \sim L^{0.4}$ for certain input parameters. These models are rather crude, and perhaps it is better to say that the (M_V, [Fe/H]) relation for dSph galaxies should be a guide for tuning the input parameters for the models of early galaxy formation.

The mean metallicity of Sextans is very similar to the other two low-luminosity dSph galaxies Draco and Ursa Minor (see review by Zinn 1992). The horizontal branch as seen in Figure 2 and in Mateo et al. (1991a) is predominantly redward of the RR Lyrae gap, with some horizontal-branch stars to the blue of the gap. At a metallicity of −2.05, the horizontal branch is extremely red and indicates that this galaxy is a "second parameter" object similar to, but perhaps not as extreme as, the dSph in Draco. Sextans certainly has a much redder horizontal branch for its metallicity than those in the distant globular clusters [R(galactocentric >7 kpc)] discussed by Lee, Demarque, & Zinn (1988). The $(B-V)/(B+V+R)$ parameter defined Lee et al. which measures the horizontal-branch morphology where B, V, and R are the number of horizontal branch stars to the blue, inside, or to the red of the RR Lyrae instability strip, is $\lesssim -0.7$ based on the data plotted in Figure 2. Insofar as age is the fundamental parameter after metallicity driving the morphology of the horizontal branch (Bolte 1989), this would indicate that Sextans, like Draco, formed its stars a few Gyr after the bulk of the Galactic globular clusters. The present photometry (Mateo et al. 1991a) can only put a lower limit of 12 Gyr on the age of the bulk of the stars in Sextans, but with deeper photometry, it may be possible to verify whether Sextans is somewhat younger than the oldest Galactic globular clusters.

The delayed formation for outer halo objects has been incorporated into a scenario for the formation of the Galaxy proposed by Searle & Zinn (1978) who hypothesized that the Galaxy formed as the coalescence of smaller subunits perhaps similar to the Magellanic Clouds. The inner subunits and the ones with very little angular momentum around the Galactic center quickly collided and merged to form the globular clusters and disk. The outer subunits however, could evolve in isolation and therefore on a much longer time scale.

The metallicity dispersion is an indicator of the chemical enrichment history of the dSph. In the simplest models of closed box evolution where there is no mass inflow or outflow, $\sigma(Z)/\langle Z\rangle$ is a constant (Mould 1984) where Z is the mass fraction of metals. We now have enough data to show that the metallicity dispersions in the dSph galaxies are not constant between galaxies. Sculptor is similar to Sextans with a dispersion of σ([Fe/H]) = 0.2 dex (Da Costa 1988). Both Draco and Fornax have apparently a significantly higher dispersion of 0.3 to 0.4 dex (Kinman, Kraft, & Suntzeff 1981; Lehnert et al. 1992; Buonanno et al. 1985). The differences in metallicity dispersions point to distinct evolutionary histories for the dSph galaxies. Such a result is not surprising in the case of Fornax and galaxies such as Carina or Phoenix where there is an old population mixed with much younger stars. But the differences in dispersion between Sextans or Sculptor and Draco also means that the galaxies which formed stars and exhausted their gas very rapidly must also have had distinct chemical enrichment histories. An obvious "enhancement" to the simple model of isolated chemical evolution which can change the ratio $\sigma(Z)/\langle Z\rangle$ is the addition of infall material to the evolving galaxy (Mould 1984).

In this simple idea of dwarf galaxy evolution in isolation, because the dissipative forces on the galaxian gas are much stronger than the dissipative forces on stars, one would expect that the later generations of stars would form kinematically "colder" material, perhaps even material in a nascent disk. If we divide our sample up into two halves [with $I > 500$ ADU and σ(vel) < 10 km s^{-1}] at metallicity [Fe/H] = −2.02, we find that the velocity dispersions are 6.1 ± 2.5 km s^{-1} ($N = 12$) and 6.3 ± 2.7 km s^{-1} ($N = 11$) for the metal-poor and metal-rich halves, respectively. There is no significant difference in velocity dispersion for the different metallicity groups, but the quality of the data may not be adequate to measure this effect.

5. THE MASS-TO-LIGHT RATIO IN SEXTANS

Using the value of the central velocity dispersion of Sextans derived in § 3 (see also Table 8), we can estimate the galaxy's mass-to-light (M/L) ratio. For this purpose, we shall adopt the

following parameters for Sextans: distance = 88 kpc; $R_c \equiv$ core radius = 15′ = 380 pc; $R_t \equiv$ tidal radius = 90′ = 2300 pc; $c \equiv \log (R_t/R_c) = 0.8$; $e \equiv$ ellipticity = 0.4; $\Sigma_{0,V} \equiv$ central V surface brightness = 26.1 ± 0.5 mag arcsec^{-2}; $S_0 \equiv$ the central luminosity surface density = 1.3 $L_\odot$ pc^{-2}; and $M_{V,\mathrm{tot}} = -9.4 \pm 0.6$.

These parameters are taken from Irwin et al. (1990) and Mateo et al. (1991a). Following Richstone & Tremaine (1986; see formulae in Mateo et al. 1991b) and a number of other studies, the basic formulae we shall employ are those for the total mass,

$$M_{\mathrm{tot}} = 167 R_c \beta v_s^2, \tag{7}$$

the central mass density,

$$\rho_0 = 166 \sigma_0^2 \eta / R_{1/2}^2 , \tag{8}$$

and the central luminosity density,

$$I_0 = S_0 / 2R_{1/2} , \tag{9}$$

of an isotropic Michie-King model (King 1966; although the equation for ρ_0 is more general as discussed by Richstone & Tremaine 1986). The parameters β and η depend on the specific model used to fit the observed surface density and velocity dispersion profiles of Sextans. An isotropic Michie-King model with $c = 0.8$ fits the data well (see Irwin et al. 1990); thus, $\beta = 7.4$ and $\eta = 0.97$. Note that equation (7) does not use the observed velocity dispersion, but rather the so-called "scale" velocity (Pryor & Kormendy 1991). This can differ significantly from the observed velocity dispersion in low-concentration systems such as Sextans. For the adopted concentration, $v_s = 1.2\ \sigma_0$, where σ_0 is the observed velocity dispersion. We adopt $\sigma_0 = 6.2 \pm 0.9$ km s^{-1}, the weighted mean listed in Table 8; therefore, $v_s = 7.4 \pm 1.2$ km s^{-1}. Pryor (1991) suggests that it is preferable to use the geometric mean radii in equations (7)–(9); consequently, we have adopted the core and tidal radii as given by Irwin et al. (1990) because they were derived using elliptically-averaged isodensity contours. For the adopted Michie-King model, $R_{1/2} = 0.8 R_c$, where $R_{1/2}$ is the radius at which the surface brightness drops to half its central value. The mean distance of the observed Sextans members from the galaxy center is $0.6 R_c$, implying a correction is less than 2% to the observed dispersion. We have therefore ignored this correction but note that it can be much larger for highly anisotropic models (e.g., Pryor & Kormendy 1990).

From equation (7) we estimate the total mass of Sextans to be $M_{\mathrm{tot}} = 2.6^{+0.8}_{-0.6} \times 10^7\ M_\odot$ where the error reflects only the contribution from the velocity dispersion uncertainty. The total luminosity of Sextans is $4.8^{+3.5}_{-2.0} \times 10^5\ L_\odot$ (we have taken $M_{V,\odot} = 4.8$); thus, $(M/L)_{\mathrm{tot}} = 54^{+44}_{-24}$. The primary contributor to the stated error is the uncertainty of the central surface brightness and not the velocity dispersion. Alternatively, using equations (8) and (9), we find $\rho_0 = 0.07 \pm 0.02\ M_\odot$ pc^{-3}, $I_0 = 2.2^{+1.6}_{-0.9} \times 10^{-3}\ L_\odot$ pc^{-3}, and $(M/L)_0 \equiv (\rho_0/I_0) = 30^{+20}_{-13}$. Armandroff & Da Costa (1986) used stellar evolutionary models to show that it is difficult to produce a pure stellar population with $(M/L)_{\mathrm{vis}}$ as large as 6.0 for a wide range of reasonable mass functions; the significantly larger mass-to-light ratios inferred for Sextans certainly cannot be interpreted in this manner.

As is the case for all the dSph galaxies studied in sufficient detail, the central velocity dispersion of Sextans is so large as to imply the existence of a considerable dark matter (DM) component. For an assumed mass-to-light ratio of the visible stars in Sextans similar to that observed in globular clusters [i.e., $(M/L) \sim 2.0$; Illingworth 1976; Pryor et al. 1991], only about 6% of the central mass density in Sextans can be accounted for from the visible material. In analogy to Draco and Ursa Minor (Pryor & Kormendy 1990; Lake 1990), Sextans therefore has barely enough visible material to cover the virial lower limit on its central mass density ($0.06\rho_0$ for a $c = 0.8$ Michie-King model; Merritt 1987; Pryor 1991). If the DM component in Sextans is less centrally concentrated than the visible material, the DM central density inferred from equation (8) should be raised by a factor 2.2 (Pryor & Kormendy 1990). In this case, the visible material only accounts for 3% of the inferred central mass density of 0.08 $M_\odot$ pc^{-3}.

The derived central dark matter density of Sextans is comparable to that inferred for Scuptor and Carina, systems at about the same Galactocentric distance as Sextans; this density is lower than that derived for the nearer Draco and Ursa Minor systems. It is tempting to attribute such a trend with Galactocentric distance to gravity, and in fact there have been attempts to use tidal models to explain the "large" velocity dispersions in these dSph galaxies. It is not apparent, however, how tidal affects could alter the *central* velocity dispersions of the dwarfs without rapidly disrupting them. We do note that Carina has a larger central luminous density than Sextans, but has a very similar M/L and central dark matter density, which naively argues against a tidal origin for the large velocity dispersions. We appeal to the community for realistic models of dwarfs orbiting much larger galaxies.

Finally, it is important to point out that we do not strictly need DM to interpret the Sextans internal kinematical results reported in this paper if many of the giants in Sextans are members of binary systems. To illustrate this, we have performed some Monte Carlo simulations of observations of populations of giant stars with varying binary fractions. Because of the large physical sizes of such stars, we have assumed that the shortest possible period is 0.5 and 1.0 yr (in accordance with observations of binary giants in globular clusters; Hut et al. 1992), while the longest period considered was 1000 yr. Such long-period binaries are unlikely to be disrupted by other Sextans members over the lifetime of the galaxy. The masses of the primary stars in the simulated binaries have been taken to be 0.8 $M_\odot$ in accordance with the evidence that the bulk of the stellar population of Sextans is quite old (Mateo et al. 1991a). Mass ratios, inclinations, ellipticities, and binary orbital phases were estimated assuming uniform probabilities for each case. The intrinsic central velocity dispersion was assumed to be 2.1 km s^{-1}, corresponding to a central mass-to-light ratio of 2.5. The results of some of these simulations are shown in Table 10. It is apparent that for binary fractions in excess of 25%, the apparent velocity dispersion can approach the observed value of 6 km s^{-1}. Thus, we cannot conclusively rule out the possibility that the central velocity dispersion of Sextans has been "artificially" inflated by binaries. The short duration of our observing run did not allow us to effectively monitor any Sextans giants for velocity variability. Comparisons of the velocities of the five stars observed in common by Da Costa et al. (1991) and ourselves about 10 months apart does not reveal any compelling evidence for binaries: only one star (number 49 in our Table 1) shows a velocity difference larger than 2 σ. Because we cannot yet rule out a binary fraction as large as 25% for the Sextans giants, we cannot conclusively interpret the central velocity dispersion results. More precise individual velocity measurements and/or better tempo-

TABLE 10

MONTE CARLO SIMULATIONS OF BINARIES[a]

P_{min} (yr)	P_{max} (yr)	f_{bin}[b]	σ_{obs} (km s^{-1})
0.5.....	1000.0	0.05	2.3
		0.10	4.4
		0.25	6.7
		0.50	9.6
1.0.....	1000.0	0.05	2.4
		0.10	3.4
		0.25	5.7
		0.50	7.6

[a] For all runs, 33 objects were sampled from a population with an intrinsic velocity dispersion of 2.1 km s^{-1}; 50 trials were performed for each set of parameters.

[b] f_{bin} refers to the binary fraction in the sense that of x apparently single stars, ($f_{bin} \times x$) are binaries.

ral coverage is necessary to settle this issue. The large sample of Sextans members identified in this study could provide the basis for such a monitoring effort.

It should be noted that the existence of binaries in the stellar population will produce a very non-Gaussian distribution of velocities, and the estimated standard deviation will be heavily weighted by the few binaries of short period. In this case, the simple estimation of standard deviation is more sensitive to the presence of binaries rather than the underlying velocity dispersion of the stellar gamma velocities. The standard deviation is not robust and other methods that clip or give low weight to deviant points should be used. Beers, Flynn, & Gebhardt (1990) list some alternative statistical measures, such as the bi-weight estimator. These methods, while giving much more robust estimates for non-Gaussian distributions, are not appropriate in the present case where the velocity error is both variable and close to the intrinsic velocity dispersion. Smaller errors of more equal weight are needed for these nonstandard estimators: in other words, higher precision velocity data will be needed to rule out binaries as the cause of the large velocity dispersion observed in Sextans.

6. SUMMARY

We have presented spectroscopic results on 80 photometrically selected stars in the direction of the Milky Way satellite dSph galaxy in Sextans. The spectra were obtained with the Argus multifiber system at the 4 m CTIO telescope in the region of the Ca II infrared triplet at 8500 Å. We have found 43 radial velocity red giant members in this galaxy and 36 field stars. Stellar metallicities were measured from $W_{8542} + W_{8662}$, the summed pseudo–equivalent widths of the two strongest Ca II triplet lines. The calibration of $W_{8542} + W_{8662}$ extends over the range $-2.2 < [Fe/H] < 0$ and is based on observations of ~270 stars in 21 Galactic and open clusters (Tables 1, 3, and 11, and Figs. 5 and 6).

The velocity of Sextans is 228 ± 1.8 km s^{-1} confirming the initial measurement of 230 ± 6 km s^{-1} by Da Costa et al. (1991). We also detect a velocity dispersion of 6.2 ± 0.9 km s^{-1}, based on the spectra of 33 stars. If we divide the data into metal-rich and metal-poor groups, we find that the velocity dispersion in each group is the same, at 6.2 ± 2.6 km s^{-1}. This velocity dispersion implies a mass-to-light ratio of $(M/L)_{tot} = 54^{+44}_{-24}$ based on isotropic, single-component King models (Illingworth 1976), or $(M/L)_0 = 30^{+20}_{-13}$ based on core-fitting techniques (Richstone & Tremaine 1986). Sextans, like the other low luminosity Milky Way dSph galaxies, evidently has a significant amount of dark matter, but until multiple epochs of velocities are determined, we cannot completely rule out binaries as the cause of the inflated velocity dispersion.

The large number of spectra of Sextans giants allows us to study the distribution of stellar metallicities of dSph stars in greater detail than before. We find that the mean metallicity of Sextans is $\langle [Fe/H] \rangle = -2.05 \pm 0.04$, with an intrinsic star-to-star metallicity dispersion of 0.19 ± 0.02 dex in [Fe/H]. We find that the metallicity based on the Ca II lines is well correlated with the color of the star on the red giant branch, supporting our claim of the detection of a real metallicity dispersion. The mean metallicity of Sextans is now in excellent agreement with the general trend of increasing metallicity with increasing galaxian absolute magnitudes for the Local Group dwarf galaxies. The low mean metallicity and red horizontal branch identify this galaxy as a "second-parameter" object similar to the dSph in Draco that may be a few Gyr younger than the metal-poor Galactic globular clusters.

The metallicity distribution of Sextans is reminiscent of the distribution of field stars in the Galactic halo, with a tail of stars extending to lower metallicities and a sharper cutoff at high metallicities. Such a distribution is qualitatively similar to a "closed box" model of chemical evolution where the galaxy evolves in isolation, followed by a period of quick removal of gas (Hartwick 1976).

We wish to thank Tad Pryor, Kyle Cudworth, Ruth Peterson, and Charles Bailyn for sending us positions, proper motions, and radial velocities for the giants in many of the galactic globular clusters studied here. We thank Francisco Valdes for for writing the Argus data reduction package in IRAF, which makes the reduction of a large number of spectra quite manageable. We thank Mark Phillips for the spectrum of star 20 that appears in Figure 10. Heather Morrison kindly supplied us with some statistical software. Edward Olszewski gratefully acknowledges partial support from NSF grants AST 86-11405 and AST 91-19343, and additional support from Dr. Peter Strittmatter. Don Terndrup acknowledges partial support from NSF grant AST 91-57038.

APPENDIX

In Table 11 we present the W values for the globular cluster giants observed by Suntzeff et al. (1992). The instrumental setup and the data reduction procedures were identical to those used for the program discussed in this paper. We have used the date in Table 11 and equation (3) to calculate the average cluster value of W' which appears in Table 2.

In Figure 10, we plot two spectra of the extremely red star 20, which is a radial velocity member of Sextans. The top spectrum was taken on 1992 May 30.97 (UT) with the CTIO 4 m telescope, RC Spectrograph, Blue air Schmidt camera, and Reticon CCD. The data have been reduced to absolute fluxes and smoothed to ~9 Å resolution. The CCD fringing and telluric absorption were

TABLE 11

PHOTOMETRY AND Ca II EQUIVALENT WIDTHS FOR PREVIOUSLY OBSERVED CLUSTERS

Star	$V-V_{HB}$	$(B-V)_0$	W (Å)	Notes
NGC 104 (47 Tucanae)				
CF2497/L2528	−0.51	1.11	5.14	
CF3116/L3512	−2.23	1.58	5.98	1
CF3133/L3708	−1.98	1.46	6.03	2
CF3208/L2605	−1.56	1.23	5.43	
CF3223/L2603	−1.16	1.25	5.59	
CF3306/L1505	−1.95	1.49	5.91	
CF3350/L1603	−2.23	1.58	6.20	
CF3420/L8624	−2.40	0.72	6.03	3
CF3579/L6527	−1.59	1.32	5.64	
CF3658/L5623	−1.85	1.39	5.92	
CF3886/L5627	−1.60	1.24	5.52	4
CF4352/L3758	−1.77	0.49	4.48	3
CF4472/L5739	−1.63	1.33	5.70	
CF4608/L7726	−2.02	1.46	5.90	2, 5
CF4615/L7701	−2.18	1.54	6.14	1
NGC 288				
A004/C38/B021	−0.28	0.87	3.72	
A007/C36/B046	−1.43	1.09	4.52	
A027/C23/B317	−0.32	0.86	3.94	
A048/—/B048	−1.86	1.18	5.28	
A056/—/B014	−0.70	0.74	3.56	4
A131/—/B180	−0.65	0.89	4.29	
A156/C41/B020	−0.82	0.91	4.48	
A188/—/B146/O340	−0.92	0.93	4.46	
A213/C20/B238	−2.30	1.33	5.10	
NGC 2692 (M67)				
S0488/IV-202	−1.71	1.53	7.07	
S1010/F141	−0.09	1.05	5.47	
S1254/F231	0.95	0.99	5.27	
NGC 1904 (M79)				
006	−0.89	0.90	3.84	
068	−2.85	1.39	5.05	
089	−1.49	0.99	4.03	
153	−2.76	1.35	4.86	
160	−3.16	1.50	4.85	
181	−2.25	1.19	4.58	
217	−1.90	1.06	4.41	
223	−3.01	1.51	5.18	
237	−2.06	1.13	4.69	
274	−1.99	1.14	4.34	
NGC 7099 (M30)				
032	−1.35	0.81	2.18	4
066	−1.16	0.90	2.60	
115	−1.79	0.88	2.69	4
171	−1.08	0.81	2.53	
PE04	−2.28	1.09	3.36	
PE10	−1.51	0.95	2.91	
PE17	−2.50	1.15	3.17	
PE18	−2.52	1.17	3.41	
PE19	−1.97	0.98	2.96	
PE23	−2.91	1.34	3.67	
PE24	−2.05	1.03	3.22	
PE91	−2.11	1.00	3.05	

NOTES.—Photometry and star identifications given in Suntzeff et al. 1992.

NOTES ON INDIVIDUAL OBJECTS.—(1) Weak TiO? (2) TiO present. (3) AGB or field star. (4) Possible AGB star. (5) Photometric variable.

removed by division by a hot star. The second spectrum was obtained by M. M. Phillips with the CTIO 1.5 m telescope and facility CCD spectrograph on 1992 December 2.32 (UT). The latter spectrum was taken under photometric conditions and corrected to wide slit fluxes, and photometry from the spectrophotometry is $R_{KC} = 16.85$ and $I_{KC} = 15.65$ with errors of 0.05 mag, based on transformations given in Hamuy et al. (1992).

The two spectra in Figure 10 show that star 20 is a variable with both Hα strongly in emission and TiO molecular absorption. The velocity of the emission line is 239 ± 20 km s^{-1}, consistent with the absorption-line velocity. The two spectra are possibly consistent with the anticorrelation of TiO absorption and Hα emission. Star 20 is within 0.2 mag of being the brightest giant in V, with $M_V = -2.3$, and given its very red colors, must be the brightest star bolometrically among this sample of Sextans giants.

Very red variable stars are quite rare in Galactic globular clusters. Rosino (1978) and Feast (1981) summarize the two general classes of red cluster variables: the Mira variables and the semiregular variables. Both types of variables are found only near the tip of the red giant branch. The Mira variables are usually defined as the variables which have light amplitudes greater than 2.5 mag. The 10 or so cluster Mira variables are confined to the metal-rich disk globulars. These stars have strong TiO bands and sometimes Hα emission. The red variables form a clear evolutionary sequence according to Feast (1981) where the variables show increasing period, Hα emission, and amplitude as they approach the red giant branch tip.

The semiregular (SR) variables form a much more heterogeneous class. Rosino (1978) has split up the SR variables into two classes: ~20 "red" semiregular variables (SR_{red}), and ~10 "yellow" (SRd), although the designation of SRd is often used for all the SR variables in globular clusters. These variables are found in both metal-rich and metal-poor clusters. Both classes of SR variables can show TiO absorption and Hα emission. Both the very red color and high luminosity identify star 20 in Sextans with the SR_{red} variables. According to Rosino (1978), these stars have periods near 100 days and $M_V \sim -2.1$. The V amplitudes are less than the Mira variables (by definition) and range from ~0.25 to 2 mag. These stars are typically the bolometrically brightest giants in the cluster. For instance, in the metal-poor cluster M53 ([Fe/H] ~ −2), the low-amplitude SR_{red} variable V50 is the brightest giant (Frogel, Persson, & Cohen 1983). In ω Cen, the two SR_{red} variables, V6 and V17, are bolometrically the brightest stars (Persson et al. 1980). V6 has TiO absorption and Hα in emission (Dickens, Feast, & Lloyd Evans 1972).

Star 20 in Sextans is evidently a member of this class of semiregular red variables. Both optical photometric monitoring as well as infrared photometry are needed to verify this classification.

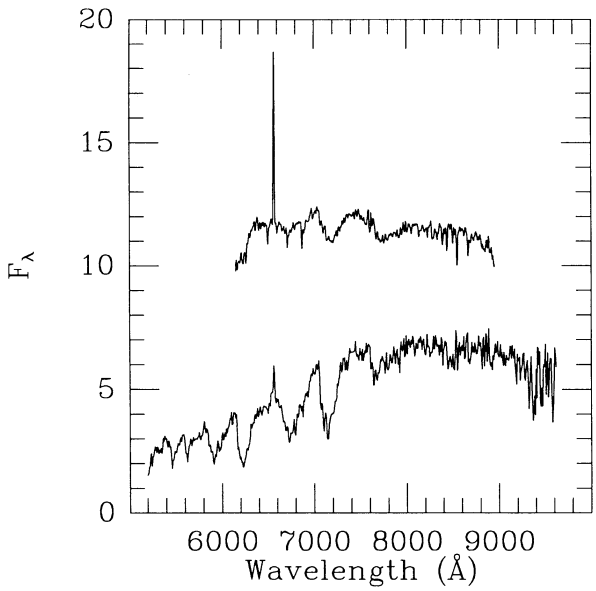

FIG. 10.—Spectrophotometry of the bright red giant member (star 20) in Sextans, taken on 1992 May 31 (*upper*) and December 2 (*lower*) with the CTIO 4 m telescope. The flux units are in units of 10^{16} ergs s^{-1} cm^{-2} $Å^{-1}$. Telluric features have been removed. The variable TiO absorption and Hα emission indicate that this star is a member of the rare class of Population II "semiregular red variables."

REFERENCES

Aaronson, M., & Olszewski, E. W. 1988, in IAU Symp. 130, Large-Scale Structures of the Universe, ed. J. Audouze, M.-C. Pelletan, & A. Szalay (Dordrecht: Kluwer), 409
Armandroff, T. E. 1989, AJ, 97, 375
Armandroff, T. E., & Da Costa, G. S. 1986, AJ, 92, 777 (AD1)
———. 1991, AJ, 101, 1329 (AD2)
Armandroff, T. E., Da Costa, G. S., & Zinn, R. 1992, AJ, 104, 164 (ADZ)
Beers, T. C., Flynn, K., & Gebhardt, K. 1990, AJ, 100, 32
Bolte, M. 1989, AJ, 97, 1688
Buonanno, R., Corsi, C. E., Fusi Pecci, F., Hardy, E., & Zinn, R. 1985, A&A, 152, 65
Caldwell, N., Armandroff, T. E., Seitzer, P., & Da Costa, G. S. 1992, AJ, 103, 840
Cannon, R. D. 1974, MNRAS, 167, 551
Chiu, L.-T. G. 1976, PASP, 88, 803
Cudworth, K. M. 1979, AJ, 84, 1866
———. 1985, AJ, 90, 65
———. 1988, AJ, 96, 105
Cudworth, K. M., & Rees, R. F. 1990, AJ, 99, 1491
———. 1991, PASP, 103, 470
Cudworth, K. M., Smetanka, J. J., & Majewski, S. R. 1992, AJ, 103, 1252
Da Costa, G. S. 1988, in IAU Symp. 126, The Harlow Shapley Symposium of Globular Cluster Systems in Galaxies, ed. J. E. Grindley & A. G. D. Philip (Dordrecht: Kluwer), 217
———. 1992, in IAU Symp. 149, The Stellar Populations of Galaxies, ed. B. Barbuy & A. Renzini (Dordrecht: Kluwer), 191
Da Costa, G. S., & Armandroff, T. E. 1990, AJ, 100, 162
Da Costa, G. S., Armandroff, T. E., & Norris, J. E. 1992, AJ, 104, 154
Da Costa, G. S. Hatzidimitriou, D., Irwin, M. J., & McMahon, R. G. 1991, MNRAS, 249, 473
Dekel, A., & Silk, J. 1986, ApJ, 303, 39
Dickens, R. J. 1972, MNRAS, 157, 299
Dickens, R. J., Feast, M. W., & Lloyd Evans, T. 1972, MNRAS, 159, 337
Dickens, R. J., & Rolland, A. 1972, MNRAS, 160, 37
Feast, M. W. 1981, in Physical Processes in Red Giants, ed. I. Iben, Jr. & A. Renzini (Dordrecht: Reidel), 193
Friel, E. D., & Geisler, D. 1991, AJ, 101, 1338
Frogel, J. A., Persson, S. E., & Cohen, J. G. 1983, ApJ, 53, 713
Gould, A., Guhathakurta, P., Richstone, D., & Flynn, C. 1992, ApJ, 388, 345
Hamuy, M., Walker, A. R., Suntzeff, N. B., Gigoux, P., Heathcote, S. R., & Phillips, M. M. 1992, PASP, 104, 533
Harris, W. E. 1975, ApJS, 29, 397
Hartwick, F. D. A. 1976, ApJ, 209, 418
Hut, P., et al. 1992, PASP, 104, 981
Illingworth, G. 1976, ApJ, 204, 73
Ingerson, T. E. 1988, in Fiber Optics in Astronomy, ed. S. C. Barden (ASP Conf. Ser., 3), 99
Ingerson, T. E., Perez, G., Schumacher, G., & Ribbeck, F. 1993, in preparation
Irwin, M. J., Bunclark, P. S., Bridgeland, M. T., & McMahon, R. G. 1990, MNRAS, 244, 16P
Jones, B. F. 1970, AJ, 75, 563
King, I. R. 1966, AJ, 71, 64
Kinman, T. D., Kraft, R. P., & Suntzeff, N. B. 1981, in Physical Processes in Red Giants, ed. I. Iben, Jr. & A. Renzini (Dordrecht: Reidel), 71
Lake, G. 1990, MNRAS, 244, 701
Lee, Y.-W., Demarque, P., & Zinn, R. 1988, in Calibration of Stellar Ages, ed. A. G. D. Philip (Schenectady: L. Davis), 149
Lehnert, M. D., Bell, R. A., Hesser, J. E., & Oke, J. B. 1992, ApJ, 395, 466
Lloyd Evans, T., & Menzies, J. W. 1977, MNRAS, 178, 163
Lutz, T. E., Ingerson, T., Schumacher, G., & Smith, D. 1990, PASP, 102, 1208
Mateo, M., Nemec, J., Irwin, M., & McMahon, R. 1991a, AJ, 101, 892
Mateo, M., Olszewski, E., Welsh, D. L., Fischer, P., & Kunkel, W. 1991b, AJ, 102, 914
Mateo, M., Suntzeff, N. B., Nemec, J., Terndrup, D., Weller, W., Olszewski, E., Irwin, M., & McMahon, R. 1992a, in IAU Symp. 149, The Stellar Populations of Galaxies, ed. B. Barbuy & A. Renzini (Dordrecht: Kluwer), 455
Mateo, M., Fischer, P., & Kzreminski, W. 1993, AJ, submitted
Mathieu, R. D., Latham, D. W., Griffin, R. F., & Gunn, J. E. 1986, AJ, 92, 1100
Menzies, J. W. 1974, MNRAS, 169, 79
Merritt, D. 1987, ApJ, 313, 121
Mould, J. R. 1984, PASP, 96, 773
Nassau, J. J., & Hynek, J. A. 1942, ApJ, 96, 37
Norris, J., Cottrell, P. L., Freeman, K. C., & Da Costa, G. S. 1981, ApJ, 244, 205
Olszewski, E. W., Schommer, R. A., Suntzeff, N. B., & Harris, H. C. 1991, AJ, 101, 515
Persson, S. E., Frogel, J. A., Cohen, J. G., Aaronson, M., & Matthews, K. 1980, ApJ, 235, 452
Peterson, R. C., Cudworth, K. M., & Rees, R. F. 1993, in preparation
Pryor, C. 1991, in Morphological and Physical Classification of Galaxies, ed. G. Longo, M. Capaccioli, & G. Busarello (Dordrecht: Kluwer), 163
Pryor, C., & Kormendy, J. 1990, AJ, 100, 127
Pryor, C., McClure, R. D., Fletcher, J. M., & Hesser, J. E. 1991, AJ, 102, 1026
Racine, R. 1971, AJ, 76, 331
Richstone, D. O., & Tremaine, S. 1986, AJ, 92, 72
Rosino, L. 1978, Vistas Astr. 22, 39
Sandage, A. 1982, ApJ, 252, 553
Schmidt, M. 1963, ApJ, 137, 758
Searle, L. 1972, in IAU Colloq. 17, Age des Etoiles, ed. G. Cayrel de Strobel & M. Delplace (Paris: Meudon Observatory), LII-1
Searle, L., & Zinn, R. 1978, ApJ, 225, 357
Suntzeff, N. B. 1992, in The Globular Cluster-Galaxy Connection; ed. J. P. Brodie & G. H. Smith (ASP Conf. Ser., 48), in press
Suntzeff, N. B., Schommer, R. A., Olszewski, E. W., & Walker, A. R. 1992, AJ, 104, 1743
Tonry, J., & Davis, M. 1979, AJ, 84, 1511

Trumpler, R. J., & Weaver, H. F. 1953, Statistical Astronomy (Berkeley: Univ. of California Press)
van den Bergh, S. 1962, AJ, 67, 486
Wheeler, J. C., Sneden, C., & Truran, J. W., Jr. 1989, ARA&A, 27, 279
Woolley, R. v. d. R., Alexander, J. B., Mather, L., & Epps, E. 1961, R. Obs. Bull., No. 43
Zaritsky, D., Olszewski, E. W., Schommer, R. A., Peterson, R. C., & Aaronson, M. 1989, ApJ, 345, 759
Zinn, R. 1992, in The Globular Cluster-Galaxy Connection, ed. J. P. Brodie & G. H. Smith (ASP Conf. Ser., 48), in press
Zinn, R., & West, M. J. 1984, ApJS, 55, 45